DESIGN OF NEW THERMALLY ACTIVATED DELAYED FLUORESCENCE MATERIALS FOR OLED APPLICATIONS USING COMPUTATIONAL CHEMISTRY

by

Rengin Büşra Özek

B.S., Chemistry, Istanbul Technical University, 2016

Submitted to the Institute for Graduate Studies in
Science and Engineering in partial fulfillment of
the requirements for the degree of
Master of Science

Graduate Program in Chemistry

Boğaziçi University

2019

DESIGN OF NEW THERMALLY ACTIVATED DELAYED FLUORESCENCE MATERIALS FOR OLED APPLICATIONS USING COMPUTATIONAL CHEMISTRY

APPROVED BY:

Assoc. Prof. Şaron Çatak .....
(Thesis Supervisor)

Prof. Viktorya Aviyente .....
(Thesis Co-supervisor)

Prof. Selmiye Alkan Gürsel .....

Prof. Alimet Sema Özen .....

DATE OF APPROVAL: 03.01.2019

ACKNOWLEDGEMENTS

First and foremost, I wish to express my genuine gratitude to my thesis supervisors Prof. Viktorya Aviyente and Assoc. Prof. Şaron Çatak for their valuable scientific guidance and support, along with their meticulous scrutiny, timely and scholarly advice had been solely responsible for completing my work.

I wish to continue my appreciation to the jury members; Prof. Selmiye Alkan Gürsel and Prof. Alimet Sema Özen for elaborately reviewing the latest manuscript and supporting remarks. I gratefully acknowledge Prof. Antonio Monari (University of Lorraine) and Dr. Seyhan Salman (Georgia State University) for their support and guidance.

I would like to thank all the Computational Chemistry and Biochemistry Group (CCBG) members for their kind help and cooperation throughout this period. I thank profusely to all my friends at Boğaziçi University, İstanbul Technical University and colleagues at Shire for their endless friendship and assistance. Finally, I am extremely grateful to my family and Emre Tugay for their eternal love, perpetual encouragement, enthusiasm and moral support.

ABSTRACT

DESIGN OF NEW THERMALLY ACTIVATED DELAYED FLUORESCENCE MATERIALS FOR OLED APPLICATIONS USING COMPUTATIONAL CHEMISTRY

This study is a theoretical assessment of thermally activated delayed fluorescence (TADF) features of fourteen molecules. The analysis based on three different descriptors; the twisting angle (α), Φ_s index and ΔE_{S-T}. The emitters are modelled by Density Functional Theory (DFT) at different levels of theories in vacuum. Conformational analyses that have been conducted at the most convenient level of theory revealed the most stable ground states geometries to be used in excited state investigations. The twisting angle (α) as a defining element of the rigidity, between donor (D) and acceptor (A) frameworks of molecules has been reported. Subsequently, the solvent effects have been taken into consideration at single point calculations in which excited state topologies have been analyzed by Time Dependent Density Functional Theory (TD-DFT) and Tamm-Dancoff Approximation (TDA) to show the charge transfer (CT) characters together with the alignment of frontier orbitals (FMOs) and ΔE_{S-T} of compounds have been introduced. Population analysis of Natural Transition Orbitals (NTOs) have been performed by TDA and Φ_s indices were reported by two different charge distributions; Löwdin and Mulliken. Lastly, the substitution effect of a conjugated moiety used for aggregation induced emission (AIE), namely AIEgens on non-TADF emitter was investigated. The descriptor analyses show that, (α) indicates the bulkiness of structures which gives rise to a highly twisted molecule with a suitable angle that directly effects the alignment of FMOs. The reported Φ_s values as indices reflecting the difference between the detachment and attachment densities, highly twisted structures have smaller values with a reduced orbital overlap which results in small ΔE_{S-T}. Note that compounds with low twisting angles have high molecular overlap densities together with large singlet-triplet band gaps.

ÖZET

OLED UYGULAMALARINDA KULLANILAN YENİ TERMAL AKTİF GECİKMELİ FLORESAN MATERYALLERİNİN HESAPSAL YÖNTEMLER İLE TASARIMI

Bu çalışma, termal aktif gecikmeli floresan (TADF) özelliği gösteren on dört molekülün üç farklı tanımlayıcıya dayanarak; bükülme açısı (α), Φ_s ve ΔE_{S-T}, yapılan kapsamlı bir teorik değerlendirmesidir. Emisyon yapan moleküller Yoğunluk Teorisi Fonksiyoneli ve farklı fonksiyoneller yardımıyla gaz fazında modellenmiştir. Farklı DFT fonksiyonel incelemelerinin arasından en uygunu seçilerek tamamlanan konformasyon analizlerinden elde edilen geometriler uyarılmış hal incelemelerinde kullanılmış olup, donör (D) ile akseptör (A) grupları arasındaki bükülmezliğin tanımlayıcı bir elemanı olan büküm açısı (α) incelenerek rapor edilmiştir. Takiben, uyarılmış hal durumları çözücü etkileri dikkate alınarak Zamana Bağlı Yoğunluk Fonksiyonel Teorisi (TD-DFT) ve Tamm-Dancoff Yaklaşımı (TDA) hesaplamaları ile yük transferi (CT) ve atomik orbitallerin molekül üzerindeki hizalanmasına ek olarak ΔE_{S-T} tetkik edilerek sunulmuştur. Doğal geçiş orbitallerinin (NTO) popülasyon analizleri TDA hesaplamaları ile gerçekleştirilmiş olup, Φ_s değerleri iki farklı yük dağılımına istinaden; Löwdin ve Mulliken, rapor edilmiştir. Son olarak, TADF özelliği göstermeyen bir materyal üzerinde konjuge yapıya sahip bir molekülün ikame etkisi incelenmiştir. Tanımlayıcı analizleri (α) değerlerinin ikame eden kalabalık yapıların moleküllere bükülme sağlayarak atomik orbitallerin dağılımını etkilediğini göstermiş olup, 0 ile 1 arasında değişken değerlere sahip ve ayrılma-eklenme yoğunlukları arasındaki fark olarak adlandırılan Φ_s değerleri, yüksek bükülme oranlarına sahip moleküllerde minimum orbital örtüşmesi ile daha düşük olup küçük ΔE_{S-T} değerlerine yol açmıştır. Düşük bükülme açılarına sahip moleküllerin orbitalleri arasındaki çakışma fazla olduğundan dolayı, enerji seviyelerinin arasındaki fark yüksek olmuştur.

TABLE OF CONTENTS

ACKNOWLEDGEMENTS iii
ABSTRACT iv
ÖZET v
LIST OF FIGURES vii
LIST OF TABLES x
LIST OF SYMBOLS xii
LIST OF ACRONYMS/ABBREVIATIONS xiii
1. INTRODUCTION 1
2. METHODOLOGY 9
2.1. Density Functional Theory 9
2.2. Time Dependent Density Functional Theory 11
2.3. Tamm-Dancoff Approximation (TDA) 14
2.4. Basis Sets 15
2.5. Continuum Solvation Models 17
2.6. Φ_s Index 18
3. AIM OF THE STUDY 22
4. RESULTS AND DISCUSSION 23
4.1. Background 23
4.2. Benchmark Calculations 24
4.3. Computational Procedure 25
4.4. Descriptor Analyses 26
4.4.1. Twisting Angle (α) 27
4.4.2. Natural Transition Orbitals 38
4.4.3. Excited State Profiles 45
4.5. Conclusion 49
5. FUTURE REMARKS 51
REFERENCES 53

LIST OF FIGURES

Figure 1.1. Structure of different OLEDs. 3

Figure 1.2. Comparision of the emission mechanisms [18]. 7

Figure 1.3. Chemical structure of PIC-TRZ. 7

Figure 2.1. Graphical description of the Φ_s descriptor as the overlap between attachment and detachment densities [53]. 20

Figure 4.1. 2D structures of TADF emitters utilized in this study. 23

Figure 4.2. Schematic representation of twisting angle [61]. 27

Figure 4.3. Optimized structure of 2CzPN as cyano-based blue emitter (M062X/6-31G(d), in vacuum). 28

Figure 4.4. Optimized structure of DMAC-DPS as sulfone-based blue emitter (M06-2X/6-31G(d), in vacuum). 28

Figure 4.5. Optimized structure of Cz2BP as benzophenone-based blue emitter (M06-2X/6-31G(d), in vacuum). 29

Figure 4.6. Optimized structure of DMAC-TRZ as 1,3,5-triazine-based blue emitter (M06-2X/6-31G(d), in vacuum). 29

Figure 4.7. Optimized structure of PXZPO as phosphine oxide-based blue emitter (M06-2X/6-31G(d), in vacuum). 30

Figure 4.8. Optimized structure of m-ATP-PXZ as 1,4-diazatriphenylene-based blue emitter (M06-2X/6-31G(d), in vacuum). 30

Figure 4.9. Optimized structure of PXZ-PXB as boron-based blue emitter (M06-2X/6-31G(d), in vacuum). 31

Figure 4.10. Optimized structure of pCBP as non-TADF emitter (M06-2X/6-31G(d), in vacuum). 31

Figure 4.11. Optimized structure of PhCz as non-TADF emitter (M06-2X/6-31G(d), in vacuum). 32

Figure 4.12. Optimized structure of TPA as non-TADF emitter (M06-2X/6-31G(d), in vacuum). 32

Figure 4.13. Optimized structure of DTT-Ox-Br as non-TADFemitter (M06-2X/6-31G(d), in vacuum). 33

Figure 4.14. Optimized structure of DTT-Ox-F as non-TADFemitter (M06-2X/6-31G(d), in vacuum). 33

Figure 4.15. Optimized structure of TPE as AIEgen fluorogen (M06-2X/6-31G(d), in vacuum). 34

Figure 4.16. Optimized structure of DTT-TPE as coupling product (M06-2X/6-31G(d), in vacuum). 34

Figure 4.17. Jablonksi Diagram for a TADF emitter. 45

Figure 4.18. Designs of Donor-Acceptor and Donor-Bridge-Acceptor Models [66]. 46

Figure 5.1. Intramolecular rotation affecting deactivation of excited TPE species [76]. 52

LIST OF TABLES

Table 4.1. Benchmark calculations of 2CzPN at different level of theories (ΔE_{S-T} in eV). 24

Table 4.2. Benchmark calculations of pCBP at different level of theories (ΔE_{S-T} in eV). 25

Table 4.3. Twisting angle (α) for TADF emitters (M06-2X/6-31G(d), in vacuum). 35

Table 4.4. Twisting angle (α) for non-TADF emitters (M06-2X/6-31G(d), in vacuum). 37

Table 4.5. Φ_s indices for TADF emitters in Lowdin (L) and Mulliken (M) charge distributions and oscillator strengths (f) (B3LYP/6-31+G(d), PCM in toluene). 39

Table 4.6. Φ_s indices for non-TADF emitters in Lowdin (L) and Mulliken (M) charge distributions and oscillator strengths (f) (B3LYP/6-31+G(d), PCM in toluene). 40

Table 4.7. Occupied and virtual NTO's for the TADF emitters (B3LYP/6-31+G(d), PCM in toluene) (1/2). 41

Table 4.8. Occupied and virtual NTO's for the TADF emitters (B3LYP/6-31+G(d), PCM in toluene) (2/2). 42

Table 4.9. Occupied and virtual NTO's for the non-TADF emitters (B3LYP/6-31+G(d), PCM in toluene) (1/2). 43

Table 4.10. Occupied and virtual NTO's for the non-TADF emitters (B3LYP/6-31+G(d), PCM in toluene) (2/2). 44

Table 4.11. Low lying singlet-triplet band gaps ΔE_{S-T} (eV) for TADF emitters (B3LYP/6-31+G(d), PCM in toluene). 47

Table 4.12. Low lying singlet-triplet band gaps ΔE_{S-T} (eV) for non-TADF emitters (B3LYP/6-31+G(d), PCM in toluene). 48

LIST OF SYMBOLS

$\mathrm{E_C}[\rho]$	Correlation energy
$\mathrm{E_X}[\rho]$	Exchange energy
$\hat{\mathrm{H}}$	Hamiltonian operator
$J[\rho]$	Coulomb energy
k_B	Boltzmann constant
$\mathrm{T}[\rho]$	Kinetic energy of interacting electrons
$\mathrm{T_s}[\rho]$	Kinetic energy of non-interacting electrons
V_{XC}	Exchange-correlation potential
α	Twisting angle
Γ	Detachment density matrix
$\Delta \mathrm{E_{S-T}}$	Singlet-triplet band gap
Λ	Attachment density matrix
$v(\mathrm{r})$	External potential
$\rho(\mathrm{r})$	Electron density
Φ_s	Quantitative Topological Descriptor

LIST OF ACRONYMS/ABBREVIATIONS

A	Acceptor
B3LYP	Becke-3-parameter Lee-Yang-Parr functional
CT	Charge Transfer
D	Donor
DF	Delayed Fluorescence
HF	Hartree-Fock
HOMO	Highest occupied molecular orbital
IP	Ionization potential
IQE	Internal Quantum Efficiency
ISC	Intersystem Crossing
ITO	Indium Tin Oxide
LUMO	Lowest Unoccupied Molecular Orbital
M06-2X	Hybrid meta exchange-correlation functional
NTO	Natural Transition Orbital
OLED	Organic Light Emitting Diodes
PCM	Polarizable Continuum Model
PF	Prompt Fluorescence
PLQY	Photoluminescence Quantum Yield
QE	Quantum Efficiency
RISC	Reverse Intersystem Crossing
SOC	Spin-orbit coupling
TD-DF	Thermally Activated Delayed Fluorescence
TDA	Tamm-Dancoff Approximation

1. INTRODUCTION

Energy is one of the prominent issues for the economic progress. However, sustainable economic growth is now being jeopardized by circumstances such as increased worldwide population that demands massive energy produced from conventional exhaustible resources. Besides, the growing energy needs give rise to the increased energy prices, reduced amounts of natural sources and harmful materials being released to the environment. Due to the greenhouse emissions caused by burning of fossil fuels such as coal, oil and natural gas, climate change issues have arisen and they bring critical consequences for social and economic infrastructure along with natural environment [1].

Despite being the largest and the most used energy source of the world, the presence of traumatic outcomes of fossil fuel usage is indisputable and day by day, the health complications arise from environmental pollutions related with greenhouse emission set barriers in front of economic growth. Still, there are alternative energy sources to eliminate the problems associated with carbon-based fossil fuel consumption. One of the aforementioned energy sources is, nuclear energy which compensates tremendous amounts of energy with no gas emissions and less quantity of resource, yet there are many speculations about the utilization of nuclear power especially in safety, reliance, toxic wastes and radiation. Nuclear power is said to have difficulties competing with other technologies due to restrictions in some countries. As a result, nuclear production started to decrease gradually soon after 2010 [1].

The most agreed difficulty of producing energy from limited resources is, maintaining the sustainability. Conserving sustainability is crucial and for a sustainable growth, governments adopt policies by taking account the provision of existing population's demands without sabotaging the capacity of next generations to fulfill their own needs [2]. According to the prevalent sights; environmental, social and economic dimensions [3] together with the flow of the resource usage and value of externalities being created [4] are the key factors of the sustainable economic growth.

The key solution to the ecological disasters, weather modifications, social and the economic crises that disrupt most nation's systems; is closely associated with sustainable growth. [5, 6]. For that reason, governments began to create solutions and novel plans based on utilization of resources and energy. As a result, large-scale of scientific studies are dedicated to understand how to use renewable energy which contributes to energy resilience through the use of hydropower, biofuels, biomass, solar energy and wind energy and emerging energy technologies such as marine energy, concentrated solar photovoltaic, artificial photosynthesis, cellulosic ethanol and enhanced geothermal energy [7]. By virtue of being an answer to the green economy and providing energy security, renewable energy is now one of the most fundamental topics of the world and a substantial increase in global renewable energy consumption and notable enlargement in renewable energy assets investments were seen in the last decade [8]. However, there are still some drawbacks such as efficiencies of the systems, production costs etc. that urgently needed to be taken care of.

Today, renewable energies compensate only 14% of the worldwide total energy supply and most of this quantity relies on conventional and unsustainable use of biomass. The advanced renewable energies' potential is strikingly greater than that of aforementioned issue. For instance, sun radiates vast amount of energy that is theoretically 15.000 times greater than earth's total energy need. Thus, it is now desired to reach to component of the above potential and leave it to the access of humankind [9–11].

At present, new technologies are being developed in order to be able to convert the energy of light to electricity effectively. Organic electroluminescence (OEL) is a phenomenon which is electrically derived emission of light from organic materials has been known for many years [12]. After the invention of electroluminescence (EL) in organic materials that inserted between two electrodes, studies about organic light-emitting diodes (OLEDs) has become widespread and OLEDs are now being used in many applications such as in smart phones, televisions, flexible displays, lightning and etc. [13]. Owing to the design flexibility, high electroluminescence efficiency, low driving voltage, fast response time, low fabrication cost and superior device performance;

OLEDs are now one of the leading topics of the display and lighting markets [13].

According to the organic layers that OLEDs have, there are various types of structures; single-layer OLED is the simplest structure that contains anode and cathode together with an organic layer which has high quantum efficiency, enhanced hole and electron transport abilities. In a two-layer OLED, one of the layers possesses the ability of transporting holes, where the other one is responsible for electron carriage. In the recombination zone, electrons-hole pair takes place and this formation gives rise to electroluminescence. In order to improve the carrier transport properties of emissive materials, an extra layer is added to the system in three-layer OLED. Insertion of an electron injection layer is seen in multi-layer OLEDs and it eliminates some important problems such as; charge carrier leakage, exciton quenching. Since excited states are usually quenched at the interface of metal and organic layer, multi-layer OLEDs which are composed of different layers namely ITO glass plate, hole injection layer (HIL), emitting layer (EML), electron transporting layer (ETL), and anode are mostly preferred for an effective electroluminescence [14]. Structures of OLEDs are shown in Figure 1.1.

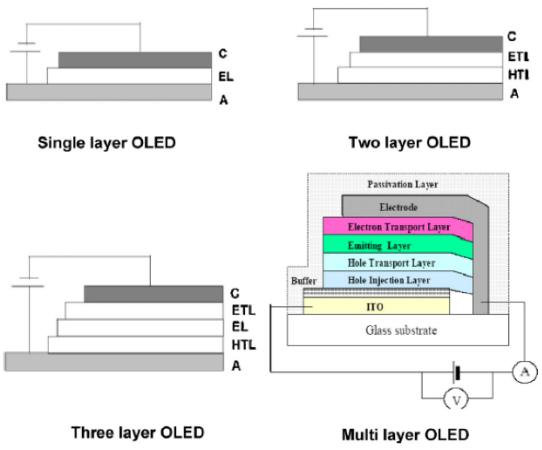

Figure 1.1. Structure of different OLEDs.

OLEDs have several advantages over liquid crystal displays (LCD) such as faster response time, greater artificial contrast ratio with wider viewing angle. Also, OLEDs are superior in terms of power efficiency and thickness [15]. However, there are some drawbacks such as high-power consumption as a result of low quantum efficiency (QE) and high driving voltage [13], and these problems lead to serious technical failures. For that reason, new methods are being developed to improve the characteristics of OLEDs, reduce the production costs in order to have competitive cost per unit with presently used technology.

As mentioned before, organic emitters used in OLED devices should also have high photoluminescence yields (PLQY). Minimized barrier to charge injection and controlled recombination zone have to be taken into account in order to enhance the quantum yield [16]. For these reasons, frontier molecular orbitals of each of the layers in device should be adjusted orderly. Recent studies demonstrate that, design of bipolar host materials that contain electron donating groups as donors (D) and electron withdrawing groups as acceptors (A) is the most prominent and effective strategy for having balanced and stable electron-hole patterns [17].

Management of hole and electron recombination is crucial because, in OLED devices energy transfer occurs from both singlet (25%) and triplet (75%) states according to the spin statistics and this phenomenon appears as a result of the exciton formation through charge recombination [18]. In addition to this, energy transfer rate is associated with the compatibility of exciton energies of donor and acceptor and according to the Dexter energy transfer (electron exchange) total spin of the donor-acceptor pair is conserved; thus, transfer of the triplet excitons is allowed [19].

Nature of spins and the emission affect lifetimes directly and nonradiative deactivation together with heat loss occurs as a result of long emission lifetimes of triplet excitons [18]. Nonradiative deactivation of triplet excitons inevitably reduces the device efficiency. As a response to this problem, Baldo *et al.* reported a novel organometallic emitter (PtOEP) that was doped into a fluorescent host and owing to the capacity of organometallic complexes to access triplet excited states through intersystem crossing

(ISC) from singlet excited state, quantum efficiencies (QE) were increasing [19].

Later on, it has been noticed that; internal quantum efficiencies (IQE) of 100% are accomplishable by the use of radiative recombination of both singlet and triplet excitons in Pt(II) and Ir(III) complexes [20]. However, application of such complexes in OLED devices has many drawbacks. For instance, rarity of heavy-metal salt reagents gives rise to a tremendous increase in costs of devices and another critical issue is environmental pollution caused by heavy-metal wastes.

To achieve commercial success and high display performances, materials used in OLED systems should have superior characteristics in a broad range of colors. Despite possessing high quantum efficiencies, organometallic complexes are not sufficient enough in blue region due to their lack of stability which directly affects color purity and brightness giving that blue pixels are labelled as the critical limitation of device performance [21]. One of the possible causes for this limitation is chemical degradation that forms charge traps that can quench excitons [22]. Bimolecular triplet-polaron annihilation (TPA) in which an energy transfer from triplets to polarons is observed and this phenomenon is responsible from the trap formation [21]. The faster degradation is explained as a consequence of highly energetic polarons, which break bonds of the molecule through thermalization [21]. Thus, highly stable and bright blue emitters are promptly needed and in response to this necessity thermally activated delayed fluorescence (TADF) molecules were introduced as the most promising exciton harvesting mechanism which is used in OLEDs, to solve the existing problems caused by TPA [18].

Soon after the first reported organic TADF emitter in 2011, studies related with TADF based OLEDs gained speed and now, with the newly synthesized highly efficient TADF emitters EQE of devices reaches up to 30% [23] together with IQE of 100% [18]. Besides being purely organic, problems related with the application of heavy-metal-based emitters do not occur in TADF-based OLEDs. The phenomenon of thermally activated delayed fluorescence is based on a small singlet-triplet energy band gap ΔE_{S-T} which is the gap between the lowest singlet energy state (S_1) and lowest triplet energy state (T_1). In theory, small energy difference (usually < 0.1 eV) between

lowest singlet state (S_1) and lowest triplet state (T_1) enables thermal up-conversion from triplet state to singlet state via reverse intersystem-crossing (RISC) [24]. In a conventional TADF molecule, two types of photoluminescence are observed; i) prompt fluorescence (PF) almost immediately in nanoseconds and there is no encounter between singlet excitons and triplet excitons, ii) delayed fluorescence (DF) where triplet excitons that were populated in triplet state via intersystem crossing (ISC) by strong spin-orbit couplings is converted back to singlet excitons by reverse intersystem crossing (RISC) [25]. To possess such an effective charge transfer, systems should contain spatially separated donor and acceptor moieties as a result of a twisted molecular structure, that leads small ΔE_{S-T} gap with fast reverse intersystem crossing rate k_{RISC}. Moreover, it should be noted that the geometrical change in a molecular conformation between ground (S_0) and the first singlet excited state (S_1) must be minimized not to cause non-radiative decay [25]. In this way, key parameters as singlet-triplet band gap (ΔE_{S-T}) RISC rate constant (k_{RISC}), ISC rate constant (k_{ISC}) should be taken into consideration when proposing new TADF emitters.

An analogy of emission mechanism of three generation is shown in Figure 1.2 [18]. In the case of 1^{st} generation, a prompt fluorescence is observed after a rapid decay of singlet excitons with an internal quantum efficiency of 25%. A large triplet phosphorescence radiative rate constant as a result of the strong spin-orbit coupling (SOC) effect between S_1 and T_1 states is observed in the case of insertion of heavy metal atoms in the 2^{nd} generation with 100% of internal quantum efficiency [26]. As mentioned earlier, 100% of internal quantum efficiency is possible due to the relatively small singlet-triplet band gap (ΔE_{S-T}) of the donor-acceptor moieties that enables an efficient charge transfer in the 3^{rd} generation.

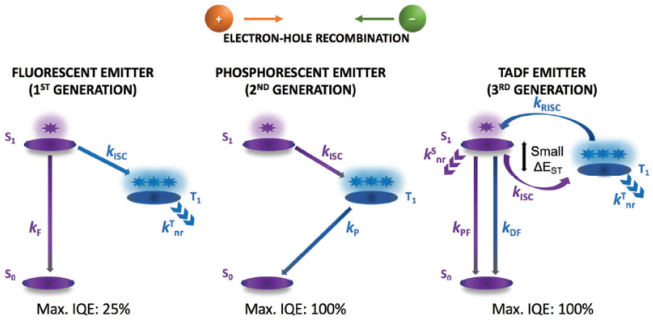

Figure 1.2. Comparision of the emission mechanisms [18].

Thereafter the first purely organic TADF emitter PIC-TRZ shown in Figure 1.3, introduced to the literature by Endo *et al.* [27], there has been an enlargement in studies related with the improvements of TADF emitters and their characteristics.

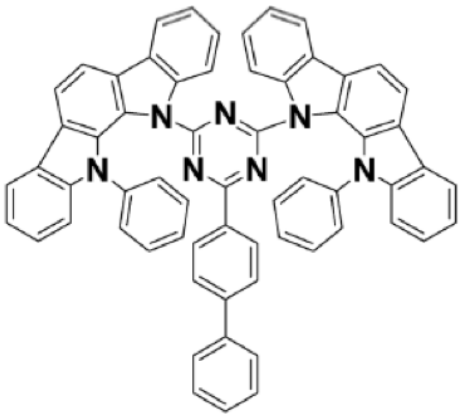

Figure 1.3. Chemical structure of PIC-TRZ.

Today, it has been reported more than a hundred new emitters with a wide range of colors: i) blue emitters are one of the most promising ones and their electroluminescence wavelength (EL_{max}) is shorter than 500 nm, ii) the electroluminescence wavelength (EL_{max}) of green-to-yellow emitters varies within the range of 500 and 580 nm and mostly they contain cyano-based acceptors, iii) orange-red emitters whose electroluminescence wavelength (EL_{max}) is longer than 580 nm are not known as blue or green emitters, yet there are many ongoing research about their improvements [18].

As a comprehensive outlook on thermally activated delayed fluorescence (TADF); for the next generation OLEDs TADF materials are considered as extremely promising candidates in terms of many advantages including remarkable device performance, low fabrication costs, easy material preparation etc. Still, the presence of some critical challenges is undeniable and through innovative strategies on designing superior TADF emitter models, it is now possible to shape the future of optoelectronics in parallel to the global demand.

2. METHODOLOGY

2.1. Density Functional Theory

Density Functional Theory which was proposed by Kohn-Hohenberg, is a quantum mechanical approach. It demonstrates that ground state (GS) and other properties of a system of electrons can be defined by optimizing electron density [28].

In particular, DFT is based on a search for exchange-correlation functional in which the electron density ρ(r) is used to describe the mixed many-body impact within a single-particle phenomenon [29]. In small systems, the exchange-correlation functional can be found exactly however it appears more inconvenient and expensive than direct solution of Schrödinger equation [30]. The description of quantum nature of matter by DFT requires the exact exchange-correlation functional. In fact, the basis of both success and failure of DFT applications is associated with the approximate nature of exchange-correlation functional [29].

Kohn stated that, for the system of many electrons where wave function methods are stopped by the exponential wall [31] and this expression is formulated in Kohn-Sham (KS) theory for the ground state energy:

$$E[\rho] = T_s[\rho] + V_{ne}[\rho] + J[\rho] + E_{XC}[\rho] \tag{2.1}$$

The kinetic energy of the noninteracting electrons is:

$$T_s[\rho] = \Sigma_i < \phi_i \left| -\frac{1}{2}\nabla^2 \right| \phi_i > \tag{2.2}$$

Where ϕ_i is the set of one electron in KS orbitals. The electron density in the KS system is defined as:

$$\rho(r) = \Sigma_i \left|\Phi_i(r)\right|^2 \tag{2.3}$$

The remaining two energy components are the nucleus electron potential energy expressed in terms of external potential $\nu(r)$ which is written as:

$$\nu(r) = -\Sigma_A \left(z_A / \left|r - R_A\right|\right) \tag{2.4}$$

$$V_{ne}[\rho] = \int \rho(r) v(r) dr \tag{2.5}$$

and the coulomb energy which is the repulsion energy between electrons $J[\rho]$ is:

$$J[\rho] = \frac{1}{2} \iint \frac{\rho(r)\rho\left(r'\right)}{|r - r'|} dr dr' \tag{2.6}$$

The sum of exchange functional $E_c[\rho]$ and the correlation functional $E_c[\rho]$ gives the exchange-correlation functional denoted as $E_{XC}[\rho]$ which includes kinetic energy term originated from the kinetic energy difference between the interacting and the non-interacting electron system. The most convenient energy contributors are, the kinetic energy term that is the measure of the freedom and exchange correlation energy in which the change of opposite spin electrons (defining extra freedom to an electron) is described [32].

The unfavorable electron-electron repulsion is depicted as Coulomb energy term hence it disfavors the total electronic energy. The electron density $\rho(r)$ can be constituted as the form of Slater determinant of one-electron functions in the Equation (2.7):

$$\rho(r) = \sum_{i=1}^{N} \langle x_i | x_i \rangle \tag{2.7}$$

The Kohn-Sham (KS) orbitals constructed by solving the Kohn-Sham equations.

$$h_i^{KS} x_i = \varepsilon_i x_i \tag{2.8}$$

Thus, the Kohn-Sham hamiltonian $\hbar_i$ is:

$$h_i^{KS} = -\frac{\nabla^2}{2} - \sum_k^M \frac{z_k}{|r_i - r_k|} + \int \frac{\rho(r)}{r_{ij}} \mathrm{d}r + V_{xc} \tag{2.9}$$

Where, V_{XC} is the exchange-correlation potential and it is in association with exchange correlation by:

$$V_{\mathrm{XC}} = \frac{\delta E_{\mathrm{XC}}}{\delta \rho} \tag{2.10}$$

As stated earlier, V_{XC} is composed of two parts: an exchange functional and a correlation functional:

$$E_{\mathrm{XC}}[\rho] = E_{\mathrm{X}}[\rho] + E_{\mathrm{C}}[\rho] \tag{2.11}$$

The interactions between the electrons of the same spin indicates the exchange term. On the other hand, the correlation term relates with interactions between the electrons of opposite spin. The exchange-correlation energy is the only unknown in Equation 2.1.

2.2. Time Dependent Density Functional Theory

One of the quantum mechanical tools utilized for the investigation of electronic excited states' natures is Time Dependent Density Functional Theory (TD-DFT). Un-

like Density Functional Theory (DFT), a much more accurate approach for numerous use-cases is presented by TD-DFT [33]. Currently, low-lying single excitations which are well predicted by TD-DFT, started to play a part in most of the technologic implementations [34]. It was possible to swiftly develop TD-DFT, which is an extension of DFT and comes with a favorable accuracy to cost ratio, into already-known codes. Hence, computing excitations via TD-DFT has become more and more preferable [33].

An alternative conceptualization of time-dependent quantum mechanics can be considered as TD-DFT whose basic variable is the one-body electron density $\rho(\boldsymbol{r}, t)$ in contrast to conventional approach that depends on wave-functions and on the many-body Schrödinger equation [35]. Since the many-body wave function is a very complex mathematical object that composed of 3N-dimensional space where N is the number of electrons in the system, it is more convenient and advantageous to use density which is a simple function that depends only on 3 variables x, y and z.

In this scope, systems are defined by the (nonrelativistic) many-body Schrödinger equation;

$$i\frac{\partial}{\partial t}\psi(\{r\}, t) = \widehat{H}(\{r\}, t)\Psi(\{\boldsymbol{r}\}, t) \tag{2.12}$$

where $\widehat{H}$ is the Hamiltonian operator and $\{\boldsymbol{r}\} = \{\boldsymbol{r}_1, \ldots, \boldsymbol{r}_\mathrm{N}\}$ are the spatial coordinates of the N electrons. Initial value problem is depicted in this equation and if the state of the system at an initial time t_0 is known, Equation 2.12 leads to calculate Ψ at any time t.

The Hamiltonian is composed of three parts;

$$\widehat{H}(\{r\}, t) = \hat{T}(\{r\}, t) + \widehat{W}(\{r\}, t) + \hat{V}_{ext}(\{r\}, t) \tag{2.13}$$

The kinetic energy term is;

$$\hat{T}(\{r\}) = -\frac{1}{2}\sum_{i=1}^{N}\nabla i^2 \tag{2.14}$$

The electron-electron repulsion is defined as;

$$\widehat{W}(\{r\},t) = \frac{1}{2}\sum_{\substack{i,j=1\\ i\neq j}}^{N}\frac{1}{|ri-rj|} \tag{2.15}$$

The third term can be written as sum of one-body potentials;

$$\hat{V}_{ext}(\{r\},t) = \sum_{i=1}^{N} v_{ext}\left(r_i,t\right) \tag{2.16}$$

Additionally, Coulomb interaction of the electrons with a set of nuclei is describes as followed;

$$v_{ext}(r,t) = -\sum_{v=1}^{N_n}\frac{Z_v}{|r-R_v(t)|} \tag{2.17}$$

Z_v and R_v are the charge and position of the nucleus respectively where v and N_n indicates the total number of nuclei in the system.

The absolute square of the wave function $\psi(\{r\},t)$ elucidated as the probability of finding one electron at r_1, another at r_2 at a given time t. Hence,

$$\rho(\boldsymbol{r},t) = N\int d^3\boldsymbol{r}_2\ldots d^3\boldsymbol{r}_N\left|\Psi\left(\boldsymbol{r},r_2\ldots\boldsymbol{r}_N,t\right)\right|^2 \tag{2.18}$$

N times of probability of finding an electron at time t and position r is given. It indicates that, the density $\rho(\boldsymbol{r}, t)$ is normalized at all times to the total number of electrons, N and it is the basic variable in terms of which TD-DFT is developed [36].

2.3. Tamm-Dancoff Approximation (TDA)

The investigation of electronic properties of large molecules became feasible by the use of Time-Dependent Density Functional Theory (TD-DFT) which is the extended version of conventional Density Functional Theory (DFT) and provides high-accuracy calculations by examining the excited state energies as well as geometries and other characteristics of large molecules with a modest computational costs compared to electron-correlated wave function methods [37]. Yet, TD-DFT is lack of success in particular points such as anticipating the excitation energies of charge-transfer states accurately, treatment of double excitations, providing the exact long-range $1/R$ dependence on donor-acceptor distance and it associates with triplet instability problems. [38–40].

Hence, the possibility to solve aforementioned issues and to have more realistic results gives rise to an increased attention on ad-hoc approximations. In this way, Tamm-Dancoff Approximation (TDA) where solely positive energy electron-hole pairs are considered, came forward with a more accurate approach [41]. Exclusively one electron-hole pair is presumed to propagate at any time interval, because in TDA the interplay between electron-hole pairs at positive and negative energies are disregarded [42].

The polarization functions can be depicted accurately by the ab-initio Bethe-Salpeter (BS) equation without being dependent on external parameters. Reduction of the non-Hermitian BS to a Hermitian problem which can be solved with stable and effective iterative methods is the major benefit of TDA [43]. In addition to providing an accurate result in singlet-triplet excitations of some unstable systems, TDA renders notable computational effort savings with relatively short operation times in contrast to TD-DFT.

As a comprehensive concept on explaining excitation energies which can be obtained as a solution of generalized eigenvalue problem:

$$\begin{pmatrix} \tilde{M} & \tilde{N} \\ \tilde{N} & \tilde{M} \end{pmatrix} \begin{pmatrix} X_p \\ Y_p \end{pmatrix} = \omega_p \begin{pmatrix} 1 & 0 \\ 0 & -1 \end{pmatrix} \begin{pmatrix} X_p \\ Y_p \end{pmatrix} \tag{2.19}$$

where X_p and Y_p are the amplitude vectors [44] and Equation 2.19 is reduced to a less complicated Hermitian problem in the case of singly excited configuration interaction thus $\widetilde{N}$ matrix elements vanishes. Hence the equation becomes;

$$\widetilde{M} X_p = \omega_p X_p \tag{2.20}$$

In this basis, the excitation energy ω_p is presented as followed;

$$\omega_p = \sum_{ai} (\epsilon_a - \epsilon_i) X_{ai}^2 + \sum_{abij} \left[\langle ib \| aj \rangle + B_{a_{i,bj}} \right] X_{ai} X_{bj} \tag{2.21}$$

The total energy for a TDA excited-state p in the case of solvent presence is;

$$G_p^{TDA} = G_{gs}^{HF} + \omega_p \tag{2.22}$$

G_{gs}^{HF} is the ground state energy and ω_p is the TDA excitation energy.

2.4. Basis Sets

Examination of atoms and molecules requires the determination of atomic and molecular wavefunctions that are generally developed from a series of one-electron one-center functions. The main necessity is that set is of sufficient size that the functions are well-represented or adjustable to be so [45].

A series of functions defining the orbitals within a system is called basis set. By adjusting computations of a range of molecules, the basis set becomes steady in a semiempirical manner. Up to the convergence is achieved, a chain of calculations with

developing basis sets is implemented. In order to have computationally feasible and economically favorable calculations, the basis set ought to be small enough because increasing number of necessary integrals diminishes the pace of calculations exponentially. Moreover, to yield more accurate outcomes within diversified geometries, the basis set shall be sufficiently flexible [45].

The basis functions are linear combination of a series of primitive Gaussian functions and splitting these primitives between different basis functions leads to a significant increase in computational efficiency [46]. The primitive exponents are shared between s and p functions for the valence functions at the split-valence level [46]. Some of the most agreed basis sets that are widely in use are 3-21G, 6-21G, 6-31+G and 6-311G* [47]. The primitives in the core functions are represented by the first number where the ones after dash indicates the number of primitives used in valance functions. The mean valence double-ζ basis is represented by two numbers where three numbers indicate the mean valence triple-ζ basis.

To provide systems with superior properties together with a more flexible mathematical computation, it is possible to add polarization functions and use extended basis set. Even though having advanced quality of electronic structure, increasing the size of basis sets results in huge computational costs at higher accuracy degrees. Moreover, to define the bigger molecular orbital occupancies diffuse functions can be supplemented. In the case of high electron densities, implementing diffuse functions which are denoted by a + sign is required. One "+" demonstrates an addition to only p orbitals where "++" is related with the addition of diffuse function to s orbitals.

Furthermore, as mentioned it is desired to get more realistic calculations to fulfill the requirement of getting the exact electronic energy, polarization functions are employed in basis sets. If the polarization considered in p orbitals which means polarization functions on non-hydrogen atoms are denoted by "*" or (d), on the contrary "**" or (d,p) indicates that polarization functions are implemented to light atoms.

2.5. Continuum Solvation Models

Solvation is an important factor in chemistry, since it affects reaction rates, pathways as well as reaction outcomes. Thus, solvent environment and its impact must be considered to the finest detail to acquire more realistic results. Despite numerous methods have been proposed for this purpose, still mimicking the solvent environment is one of the significant challenges in molecular modeling [48].

In the Quantum Mechanical (QM) approach, the solvent effects are defined by conceptual models called as continuum solvation models in which the number of degrees of freedom are defined continuously through the agency of distribution function [49].

The solvent environment is depicted as a polarizable medium portrayed by its static electric constant ε and the solute is embedded in a cavity enclosed by dielectric atmosphere. Equation 2.23 clarifies the total solvation free energy,

$$\Delta G_{\text{ solvation}} = \Delta G_{\text{cavity}} + \Delta G_{\text{dispersion}} + \Delta G_{\text{electrostatic}} + \Delta G_{\text{repulsion}} \tag{2.23}$$

the energetic cost of implementing the solute in the medium is represented by ΔG_{cavity}, where $\Delta G_{dispersion}$ is associated with the dispersion interactions takes place between solvent and solute and it supplies stabilization to solvation free energy. The constituent of the solute-solvent interaction energy is $\Delta G_{electrostatic}$. The final fragment of the equation $\Delta G_{repulsion}$ implies the exchange solute-solvent interactions which is not incorporated in the cavitation energy.

The electrostatic problem which is the primary weak spot of the continuum solvation model, is identified by the Poisson equation.

$$-\vec{\nabla}[\varepsilon(\vec{r})\nabla\vec{V}(\vec{r})] = 4\pi\rho_M(\vec{r}) \tag{2.24}$$

$$-\nabla^2 V(\vec{r}) = 4\pi\rho_M(\vec{r}) \text{ within } C \tag{2.25}$$

$$-\varepsilon\nabla^2 V(\vec{r}) = 0 \text{ outside } C \tag{2.26}$$

Portion of the space occupied by cavity is denoted as C, where ε is dielectric function, total quantity of electrostatic potential constituted by charge distribution ρ_M. The reaction potential produced by the polarization of the dielectric medium is:

$$V(\vec{r}) = V_M(\vec{r}) + V_R(\vec{r}) \tag{2.27}$$

The class of polarizable continuum solvation models comprises the polarizable continuum model (PCM) in which the solute is inserted in a cavity described by a group of spheres centered on atoms with a radii portrayed by the van der Waals radius of the atoms multiplied by a predefined factor (usually around 1.2) [50]. Then, the subdivision of the cavity surface into small domains called as tesserae is observed where the polarization charges are placed. PCM calculations can be performed by various approaches. Dielectric PCM (D-PCM) is the preliminary method where Conductor-like PCM (C-PCM) is the second model in which enclosing environment is considered as a conductor in place of dielectric, and the last method is a practice by means of the PCM equations altered in an integral equation formalism (IEF-PCM) [51].

2.6. Φ_s Index

Assessment of the charge-separation features of chromophores is crucial to understand the effectivity of the charge transfer upon the light absorption that takes place in the chromophore. For this purpose, a quantum mechanical descriptor of photoinduced electronic charge density variation namely Φ_s index, was developed to quantitatively evaluate the magnitude of the charge separation [52].

The Φ_s index, accounts for a consistent diagnostics tool for xc-functionals, theoretically interpreted as the spatial overlap between the detachment and the attachment densities [52]. Since, Φ_s index associates with the investigation of density matrices, it is possible to get density matrices related to ground state (P_0) and to the X^{th} excited state (P_x) from the excited state calculations. Hence, the difference density matrix Δ

is obtained as:

$$\Delta = P_X - P_0 \Rightarrow \sum_{k=1}^{K} (\Delta S)_{kk} = 0 \tag{2.28}$$

If the system does not contain any electron exchange, the entropy change ΔS, is the difference in entropy between to states of a system equals to zero. The eigenvalues of Δ in the diagonal matrix δ can therefore be provided by unitary similarity transformation that is performed on Δ.

$$\exists U \left| \delta = U^{\dagger} \Delta U; \quad (\delta)_{ij} = 0 \quad \forall \quad i \neq j \right. \tag{2.29}$$

Detachment/attachment orbitals can be obtained from diagonalizing the Δ [53]. Δ has either positive or negative eigenvalues. Subsequently, two novel diagonal matrices $\sigma+$ and σ- can be presented and their constituents are the functions of δ. These diagonal matrices are utilized for the acquisition of Detachment Γ and Attachment Λ density matrices. The insufficient electron density originates from light absorption is demonstrated by detachment, where the increments of electron density at excited state is represented by attachment. Since there is no electron loss along the vertical excitation, it can be seen that the density matrices can be expressed in the space of K atomic orbitals:

$$\sum_{\mu=1}^{K} (\Gamma S)_{\mu\mu} = \sum_{\mu=1}^{K} (\Lambda S)_{\mu\mu} \tag{2.30}$$

Accordingly, it is possible to portray the associated detachment/attachment densities in 3D space:

$$\varrho_\tau\left(\xi_1,\xi_2,\xi_3\right)=\sum_{\mu=1}^{K}\sum_{v=1}^{K}(\tau)_{\mu v}\varphi_\mu\left(\xi_1,\xi_2,\xi_3\right)\varphi_v\left(\xi_1,\xi_2,\xi_3\right) \tag{2.31}$$

$$\tau=\Gamma,\Lambda \tag{2.32}$$

where ξ_1,ξ_2,ξ_3 are three spatial coordinates. The spatial distribution of the electronic density removed (detachment) from the ground state and reconstructed (attachment) in excited states in the course of the transition, demonstrated by two aforementioned functions. Remarkably, the detached/attached charged can be represented as:

$$\vartheta_\tau=\int_R d\xi_1\int_R d\xi_2\int_R d\xi_3\varrho_\tau\left(\xi_1,\xi_2,\xi_3\right)\equiv\int_{R^3}d^3\xi\varrho_\tau(\xi) \tag{2.33}$$

As a result, the overlap between attachment and detachment densities denoted as dimensionless Φ_s index can be portrayed as:

$$\phi_s=\vartheta^{-1}\int_{R^3}d^3\xi\sqrt{\varrho_\Gamma(\xi)\varrho_\Lambda(\xi)} \tag{2.34}$$

The Φ_s index is linked with the charge-transfer of the electronic transition and it varies within the range of 0 and 1. In the case of absolutely no overlap between detachment and attachment matrices, Φ_s then be equal to 0. It equals to 1 in severe cases where there is no fluctuation between ground and excited states.

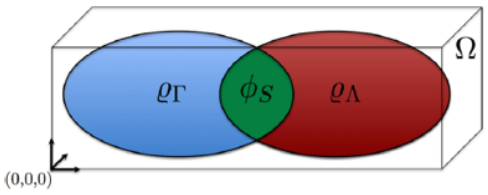

Figure 2.1. Graphical description of the Φ_s descriptor as the overlap between attachment and detachment densities [53].

It is noteworthy to state that, the detachment and attachment densities will be integrated over the delimited volume Ω from a three-dimensional integration grid encircling the chromophore as in the Figure 2.1.

The calculated Φ_s indices in this study belong to two different charge distribution analyses; Löwdin and Mulliken where negative values can be obtained from Mulliken populations that are overly affected by basis sets, on the other hand alteration of all the atomic orbitals to an orthogonal basis is utilized in Löwdin populations [54, 55]. The overlap population is equally separated between two atoms of a bond in Mulliken analysis, leading to a simpler approach. But this approximation may cause unrealistic values in some cases. Thus, to address the problems associated with Mulliken populations, Löwdin charge distribution in which the atomic orbitals are converted to an orthogonal basis set, is used to have an advanced population analysis [56].

3. AIM OF THE STUDY

In this study, investigation of the relationship between molecular structures as well as photophysical properties of a range of emitters was accomplished to stimulate a strategy for designing suitable molecular structures by quantum calculations. To understand the correlation between the molecular structure and TADF property, a comparative study was held among the molecules that possess TADF features and structures which are poor in TADF characteristics. Seeing that the blue-emitter complexes are not satisfactory in terms structural and operational deficiency, characteristics of blue emitters with a various subgroup was examined via three different descriptors to make a comparison with non-TADF structures in this study. The descriptors are namely; twisting angle (α) between the adjacent electron donating (D) and electron accepting (A) units, band gap (ΔE_{S-T}) between the lowest lying singlet (S_1) and triplet (T_1) state and Φ_s index which demonstrates the overlap between attachment and detachment densities

To elucidate the subgroups of blue emitters concisely; DMAC-DPS is based on a diphenyl sulfone as acceptor, Cz2BP contains benzophenone, DMAC-TRZ includes 1,3,5-triazine, *m*-ATP-PXZ as 1,4-diazatriphenylene based, 2CzPN as cyano based and PXZ-PXB as boron based.

This study also includes a cross comparison of a group of non-TADF molecules namely as pCBP, PhCz, TPA, TPE, DTT-*s*,*s*-dioxide [57] and a coupling product of DTT-*s*,*s*-dioxide with TPE namely as 3,5-Bis(4'-(1,2,2-triphenylvinyl)-[1,1'-biphenyl]-4-yl)dithieno[3,2-b:2',3'-d]thiophene-4,4-dioxide to blue emitters. By enlightening the differences of optoelectronic properties, a design strategy for novel emitters is intended to be offered as the main objective of the work.

4. RESULTS AND DISCUSSION

4.1. Background

Thermally activated delayed fluorescence (TADF) emitters have drawn attention recently since they effectively give rise to the replacement of singlet excitons into triplet excitons. Utilizing traditional organic compounds in emitters boost the electroluminescence (EL) efficiency of organic light emitting diodes (OLEDs) [58]. In the absence of noble metals in contrast to phosphorescence emitters, TADF emitters can achieve high internal quantum efficiencies (IQE) thus they are extremely innovative.

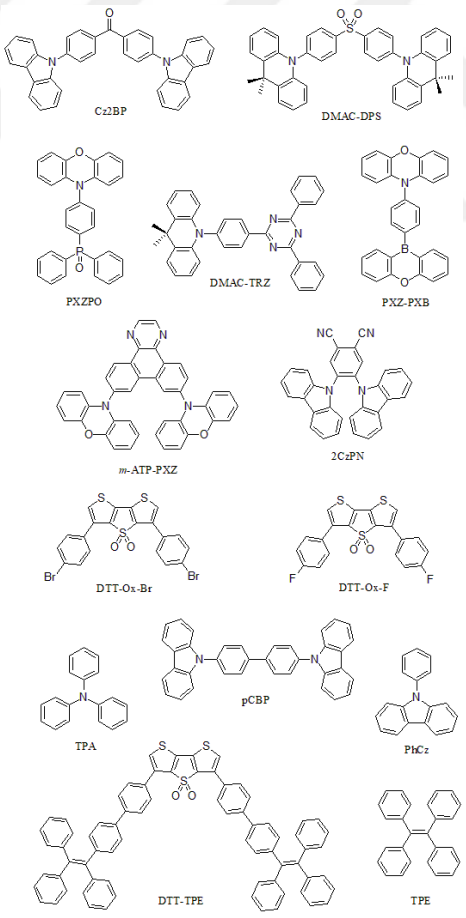

Figure 4.1. 2D structures of TADF emitters utilized in this study.

4.2. Benchmark Calculations

The precision of theoretical studies is highly dependent on the methodology in which molecular orbitals are introduced. Thus, in this study a group of functionals and basis sets were examined to reach more consistent singlet and triplet energies with experimental data.

To find the energetically favored geometries of the emitters, optimizations at different levels of theories (M06-2X, B3LYP) and basis sets (6-31G(d), 6-31G+(d)) are accomplished. Conformation analyses are performed by changing the dihedral angles of each molecule. The effects of each conformer on band gap are examined by Boltzmann Distribution and it is observed that most significant contribution is obtained from the conformers that have the lowest energy in kcal relatively.

Ground state calculations at different levels of theories showed that the most realistic geometries are obtained at M06-2X/6-31G(d) in vacuum where, the benchmarking calculations for TADF emitter 2CzPN (Table 4.1) and non-TADF emitter pCBP (Table 4.2) revealed the most consistent excited state energies to be the ones computed at B3LYP functional with 6-31+G(d) basis sets in a shorter time frame by Time Dependent Density Functional Theory and Tamm-Dancoff Approximation (TDA).

Table 4.1. Benchmark calculations of 2CzPN at different level of theories (ΔE_{S-T} in eV).

Functional/Basis Set	**TD-DFT**	**TDA**	**Exp.**
M06-2X/6-31G(d) in vacuum	0.51	0.45	0.31
B3LYP/6-31G(d) in vacuum	0.32	0.27	
B3LYP/6-31G(d) in toluene	0.29	0.25	
B3LYP/6-31+G(d) in vacuum	0.31	0.27	
B3LYP/6-31+G(d) in toluene	0.28	0.24	

Table 4.2. Benchmark calculations of pCBP at different level of theories (ΔE_{S-T} in eV).

Functional/Basis Set	**TD-DFT**	**TDA**	**Exp.**
M06-2X/6-31G(d) in vacuum	0.74	0.67	0.25
B3LYP/6-31G(d) in vacuum	0.59	0.46	
B3LYP/6-31G(d) in toluene	0.60	0.45	
B3LYP/6-31+G(d) in vacuum	0.56	0.45	
B3LYP/6-31+G(d) in toluene	0.57	0.44	

Additionally, solvent effects are analyzed in excited state calculations to imitate reaction conditions by Polarizable Continuum Model (PCM) in toluene. Since TDA yields more stable triplet states and band gaps closer to experimental data, further calculations are continued by employing TDA and reported singlet-triplet band gaps belong to this approach.

4.3. Computational Procedure

The optimizations of ground and excited state geometries together with a conformational analysis are used to locate the most stable and energetically favorable geometries. Optimizations of ground states geometries are carried out at the M06-2X and B3LYP levels with 6-31G(d) and 6-31+G(d) basis sets. Being a type of hybrid meta exchange-correlation functional, M06-2X is a high-nonlocal functional and parametrized for solely nonmetals [59]. To clarify the most stable and suitable molecular structures, B3LYP, which is the most commonly employed functional due to its higher performance in energy evaluations, was also employed [60]. Despite being effective, B3LYP has some malfunctions in defining energies, reaction barrier heights and larger molecules [60]. Geometries optimized at the M06-2X/6-31G(d) level in vacuum are predicted well and these optimized geometries are taken to further model the excited state topologies and metrics at several functional/basis set combinations including

M06-2X/6-31G(d), B3LYP/6-31G(d) both in vacuum and solvent. The solvent effects are examined using polarizable continuum method (PCM) in toluene [49].

To quantify the charge transfer (CT) character of the electronic transitions and the natures of excited states, natural transition orbitals (NTOs) analysis are conducted to evaluate Φ_s index, a quantum mechanical descriptor associated with the electronic cloud polarization and portrays the photoinduced electronic charge density variation numerically. [61]. The electron density transported from ground state is known as detachment density ($\varrho\Gamma$) and its reconstituted form in the excited state is acknowledged as attachment density ($\varrho\Lambda$). Φ_s value obtained from analyses are in the range of 0, which implies charge transfer with minor overlap, and 1 that indicates a local transition with a high overlap. The Φ_s indices and together with occupied and virtual Natural Transition Orbital depictions are assessed by using NANCY_EX_2.0 software package [52]. All the calculations at ground and excited states were performed at Gaussian 09 program package [62].

4.4. Descriptor Analyses

Luminescence properties such as color, intensity and emission lifetime of organic luminescent materials, by means of molecular structural design, can be managed provided boundless improved implementations in electroluminescence, organic lasers, sensors and bioimaging [63]. However, as mentioned earlier in the previous sections, devices suffer from low quantum efficiencies and lifetimes, color instabilities etc. To address these issues, many strategies have been developed and TADF is one of them. Still, there are various spots which need to be highlighted when designing innovatory materials that dominate sophisticated TADF characteristics.

To understand why a material shows TADF properties and how these characteristics can be improved, a comparative study has been performed through the investigation of three different descriptors namely i) twisting angle (α), ii) ΔE_{S-T} the band gap between the lowest singlet excited state (S_1) and triplet state (T_1), iii) Φ_s index which is obtained from natural transition orbital analyses to accentuate the structural

differences that affect TADF characteristics of molecules.

4.4.1. Twisting Angle (α)

When designing TADF emitters, minimizing the gap between the excited states is emphasized. To satisfy this need, one can arrange the positions of adjacent donors and acceptors with a suitable dihedral angle that enables torsion to the whole molecule, also entitled as twisting angle (α).

In order to have an adequate amount of spatial separation of HOMO and LUMO which gives rise to a small ΔE_{S-T}. This is possible with the introduction of steric hindrance which causes large twisting angle to the molecule [58]. Since the charge transfer through the entire molecule is governed by twisting angle, photophysical properties of those emitters such as radiative and nonradiative decay rates denoted as k_r and k_{nr} respectively, depend upon α [58, 64]. In general, TADF emitters are designed by implementing the planar donor and acceptor groups because maintaining highly twisted links between moieties, donor and acceptor groups should have a rigid structure that enables bulkiness [65].

Below, Figure 4.2 shows a general view of twisting angle between two moieties as a key parameter.

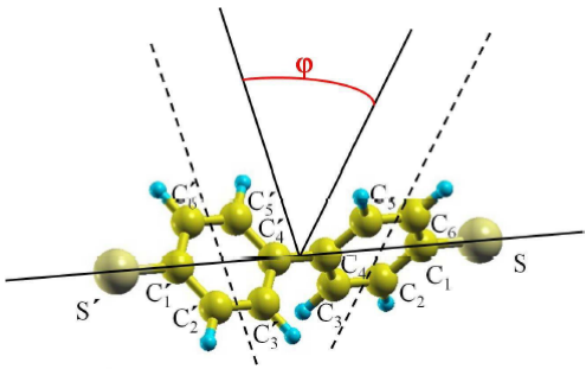

Figure 4.2. Schematic representation of twisting angle [61].

3D structures of TADF and non-TADF emitters studied in this thesis are shown in Figures 4.3 - 4.16.

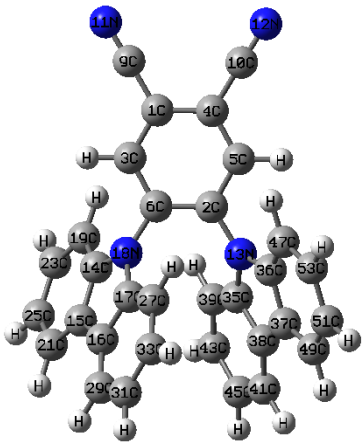

Figure 4.3. Optimized structure of 2CzPN as cyano-based blue emitter (M062X/6-31G(d), in vacuum).

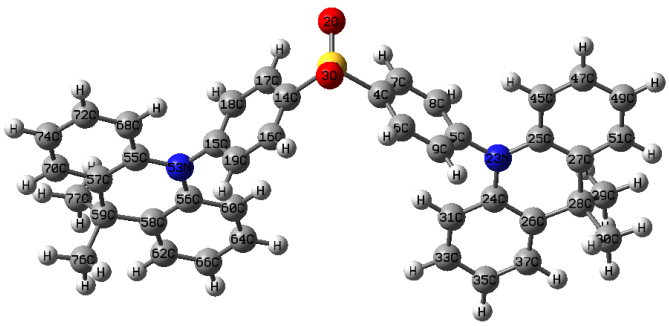

Figure 4.4. Optimized structure of DMAC-DPS as sulfone-based blue emitter (M06-2X/6-31G(d), in vacuum).

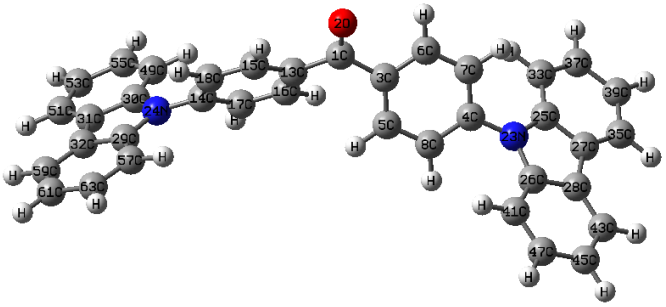

Figure 4.5. Optimized structure of Cz2BP as benzophenone-based blue emitter (M06-2X/6-31G(d), in vacuum).

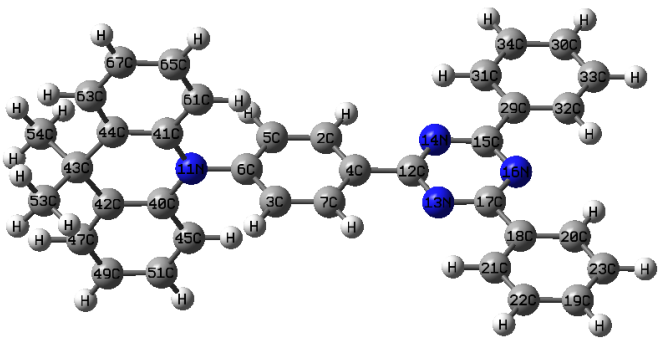

Figure 4.6. Optimized structure of DMAC-TRZ as 1,3,5-triazine-based blue emitter (M06-2X/6-31G(d), in vacuum).

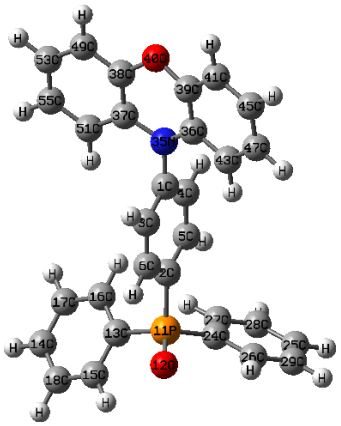

Figure 4.7. Optimized structure of PXZPO as phosphine oxide-based blue emitter (M06-2X/6-31G(d), in vacuum).

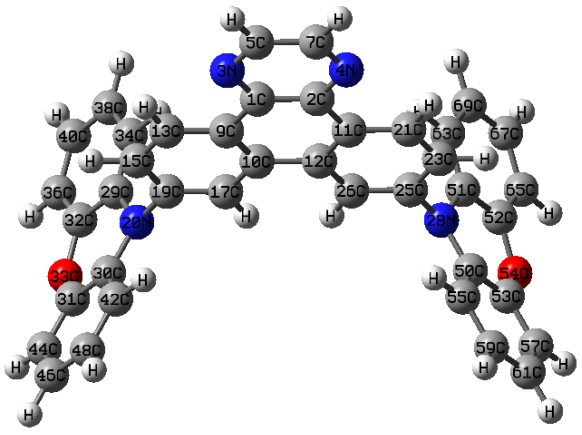

Figure 4.8. Optimized structure of m-ATP-PXZ as 1,4-diazatriphenylene-based blue emitter (M06-2X/6-31G(d), in vacuum).

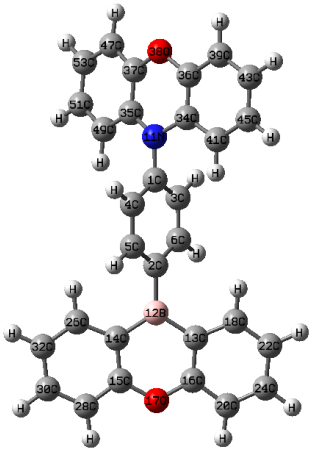

Figure 4.9. Optimized structure of PXZ-PXB as boron-based blue emitter (M06-2X/6-31G(d), in vacuum).

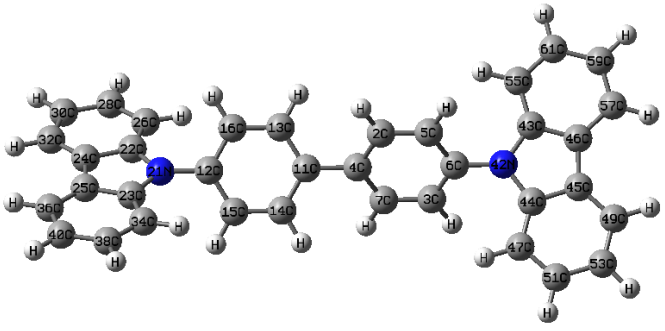

Figure 4.10. Optimized structure of pCBP as non-TADF emitter (M06-2X/6-31G(d), in vacuum).

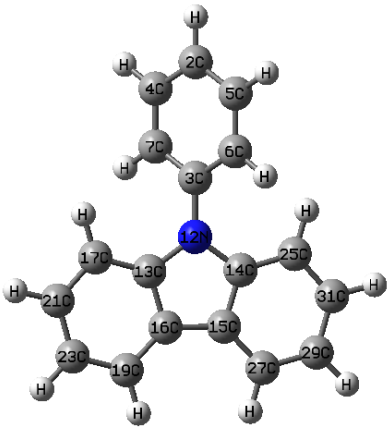

Figure 4.11. Optimized structure of PhCz as non-TADF emitter (M06-2X/6-31G(d), in vacuum).

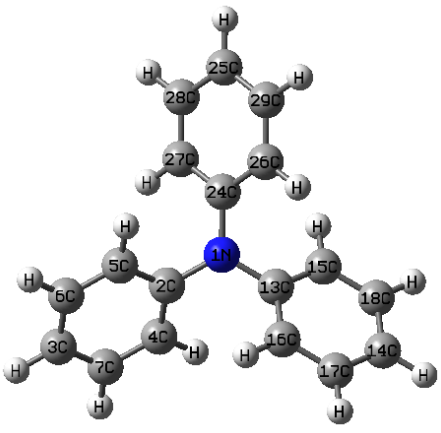

Figure 4.12. Optimized structure of TPA as non-TADF emitter (M06-2X/6-31G(d), in vacuum).

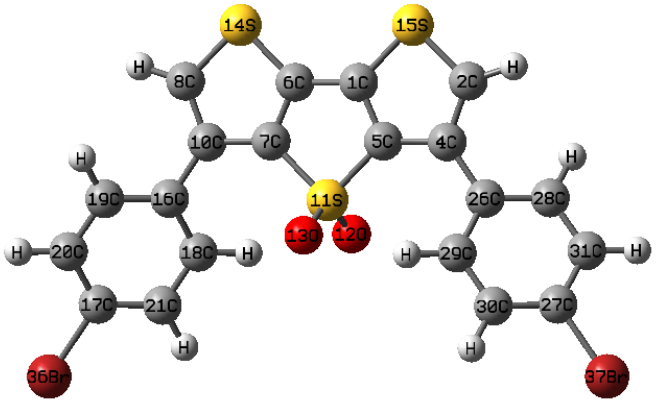

Figure 4.13. Optimized structure of DTT-Ox-Br as non-TADFemitter (M06-2X/6-31G(d), in vacuum).

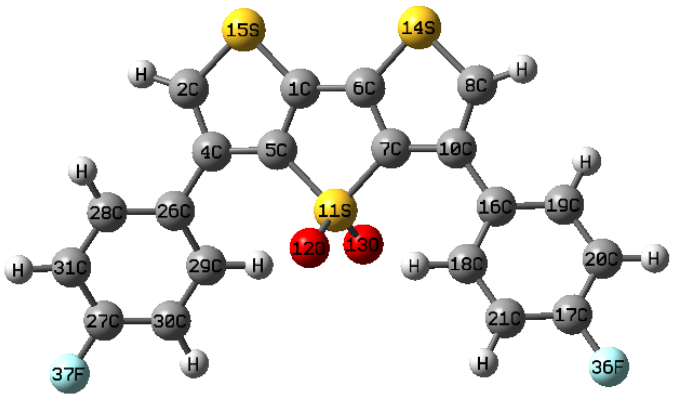

Figure 4.14. Optimized structure of DTT-Ox-F as non-TADFemitter (M06-2X/6-31G(d), in vacuum).

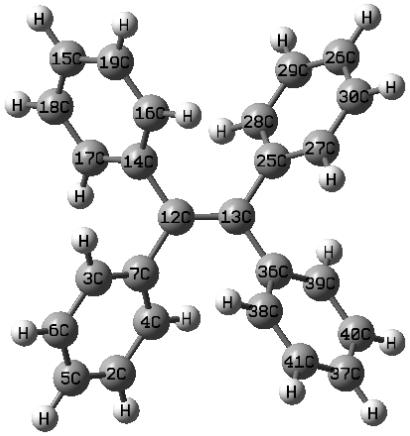

Figure 4.15. Optimized structure of TPE as AIEgen fluorogen (M06-2X/6-31G(d), in vacuum).

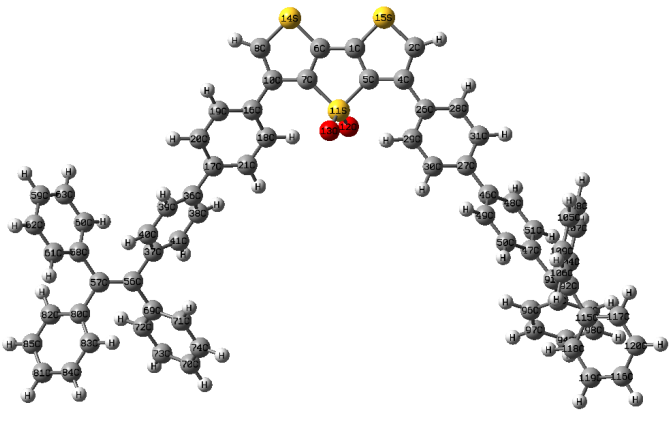

Figure 4.16. Optimized structure of DTT-TPE as coupling product (M06-2X/6-31G(d), in vacuum).

Table 4.3. Twisting angle (α) for TADF emitters (M06-2X/6-31G(d), in vacuum).

Compound	**Atoms**	α
2CzPN	C5-C2-N13-C36	60.01
	C3-C6-N18-C14	60.01
DMAC-DPS	C8-C5-N23-C25	87.7
	C19-C15-N53-C56	-94
Cz2BP	C7-C4-N23-C25	-49.73
	C17-C14-N24-C30	-49.15
DMAC-TRZ	C3-C6-N11-C40	-90
PXZPO	C37-N35-C1-C4	97.17
	C36-N35-C1-C3	73.96
m-ATP-PXZ	C23-C25-N28-C50	72.68
	C17-C19-N20-C30	107.83
PXZ-PXB	C3-C1-N11-C34	-80.84
	C4-C1-N11-C34	99.01

Twisting angles between donor (D) and acceptor (A) are given in Table 4.3. 2CzPN (Figure 4.3) with 60.01^o dihedral angle, is a type of cyano-based materials that is one of the widespread building blocks used in TADF emitters. Relatively low dihedral angle is related with the absence of steric hindrance and bulkiness in 2CzPN. This effect is observed as a large band gap between the excited states. It is possible to induce more effective RISC between two excited states by introducing higher rigidity to the molecule by attaching large groups that provides higher twisting angle.

The same condition is valid for a benzophenone-type acceptor Cz2BP (Figure 4.5) that has -49.73^o of twisting angle. Thus, more sterically hindered versions with *ortho*-carbazole substitutions of Cz2BP are reported in the study of Wong *et al.* [18] and increased torsion between donor and acceptor moieties gives rise to a more suitable twisting angle together with a relatively small band gap.

The selection of dimethylacridan (DMAC) as donor in two emitters; DMAC-DPS (Figure 4.4) sulfone-based and DMAC-TRZ (Figure 4.6) 1,3,5-triazine-based structures, gives steric hindrance and leads to a larger twisting angle.

As in the case of PXZPO (Figure 4.7) in which phosphine oxide was utilized as weak acceptor, the angle indicates a moderate torsion between D and A units.

The emitter constructed from 1,4-diazatriphenylene acceptor *m*-ATP-PXZ (Figure 4.8) shows compatible twisting angle of 72.68^o with its band gap due to the powerful donor phenoxazine (PXZ). Additionally, the last TADF emitter PXZ-PXB (Figure 4.9) built with boron-based acceptor has suitable twisting angle as a result of a torsion between phenoxazine donor and boron-based acceptor.

Non-TADF emitters and their dihedral angles are listed in the Table 4.4 All the molecular designs above are based on an absence of twisted conformation and steric hindrance; therefore, their dihedral angles are not suitable to provide separation of donor and acceptor moieties.

Table 4.4. Twisting angle (α) for non-TADF emitters (M06-2X/6-31G(d), in vacuum).

Compound	**Atoms**	α
pCBP	C16-C12-N21-C22	52.7
	C3-C6-N42-C44	-51.49
PhCz	C7-C3-N12-C13	-52.07
	C6-C3-N12-C14	-52.07
TPA	C4-C2-N1-C13	-39.24
	C27-C24-N1-C13	141
DTT-Ox-Br	C8-C10-C16-C19	-32.69
	C2-C4-C26-C29	146.89
DTT-Ox-F	C8-C10-C16-C19	-33.34
	C2-C4-C26-C29	146.02
TPE	C14-C12-C7-C3	-47.36
DTT-TPE	C31-C27-C46-C48	33.76
	C20-C17-C36-C38	143.99

The emitters are shown in Table 4.4 emit light however, the RISC being an endothermic process is not assisted due to a strictly increased ΔE_{S-T} as a consequence of non-interrupted π-conjugation. Thus, the dihedral angle and separation distance of moieties implicitly affects color purity and singlet-triplet energy splitting together which is a vital point in designing effective emitters.

It is worth to note that, all the non-TADF emitters lack suitable twisting and orbital separation, on the other hand an effective TADF emitter can be designed by substitution of these moieties to suitable donor or acceptor structures. For instance, triphenylamine (TPA) group is a significant electron-donating group that is utilized for many research disciplines and it is used as building blocks to provide a precise twisting to the molecule. The same condition is valid for tetraphenylethylene (TPE) that is also constructed in the coupling product DTT-TPE (Figure 4.16). TPE is one of the building materials that is used to generate an emission by causing aggregates. This formation is named as Aggregation Induced Emission (AIE) and it effectively increases the quality of the emission by restricting the existed intramolecular rotation within the molecule so that the excess energy is dissipated as light. Additionally, a decrease in singlet-triplet energy splitting was observed for the coupling product. However, a considerable change was not observed for twisting angle. The reduction in the band gap is probably due to the aggregation induced emission effect which is explained in detail in the subsequent topic.

4.4.2. Natural Transition Orbitals

To identify the distinction between a TADF emitter and a non-TADF material, the molecular orbitals responsible for the charge transfer should be well aligned in order to induce exciton transformation from T_1 to S_1 effectively.

Separated HOMO and LUMO for TADF process is essential and emission is supported by D-A molecular frameworks which present intermolecular charge transfer (CT) character. An efficient reverse intersystem crossing (RISC) process within TADF materials is related with a reduced overlap between frontier orbitals where small overlap

(a) is desired to have CT.

Hereby, natural transition orbital formalism which diagonalize the transition density matrix, is proposed to give better explanation of the excited state characteristics [66].

The Φ_s index being the explanation of the overlap density between detachment and attachment matrices, is listed in Table 4.5 and Table 4.6, ranging from 0 to 1.

Table 4.5. Φ_s indices for TADF emitters in Lowdin (L) and Mulliken (M) charge distributions and oscillator strengths (f) (B3LYP/6-31+G(d), PCM in toluene).

Compound	**Transition**	**L**	**M**	**f**
2CzPN	$S_0 \rightarrow S_1$	0.4862	0.5480	0.0793
DMAC-DPS	$S_0 \rightarrow S_1$	0.1459	0.2490	0.0006
Cz2BP	$S_0 \rightarrow S_1$	0.4515	0.4869	0.48
DMAC-TRZ	$S_0 \rightarrow S_1$	0.0078	0.0093	0.00
PXZPO	$S_0 \rightarrow S_1$	0.2664	0.4869	0.0041
m-ATP-PXZ	$S_0 \rightarrow S_1$	0.1272	0.2128	0.0049
PXZ-PXB	$S_0 \rightarrow S_1$	0.1935	0.2737	0.0025

Table 4.6. Φ_s indices for non-TADF emitters in Lowdin (L) and Mulliken (M) charge distributions and oscillator strengths (f) (B3LYP/6-31+G(d), PCM in toluene).

Compound	**Transition**	**L**	**M**	**f**
pCBP	$S_0 \rightarrow S_1$	0.6426	0.7021	0.82
PhCz	$S_0 \rightarrow S_1$	0.8271	0.8619	0.05
TPA	$S_0 \rightarrow S_1$	0.6318	0.6662	0.02
DTT-Ox-Br	$S_0 \rightarrow S_1$	0.7437	0.7579	0.36
DTT-Ox-F	$S_0 \rightarrow S_1$	0.7567	0.7826	0.36
TPE	$S_0 \rightarrow S_1$	0.7980	0.7856	0.54
DTT-TPE	$S_0 \rightarrow S_1$	0.6895	0.7400	0.02

The Φ_s indices for TADF emitters in Table 4.5 and for non-TADF emitters in Table 4.6 reveals the charge transfer characters of molecules. Φ_s indices computed for TADF emitters are closer to 0 displaying a reduced overlap between detachment and attachment densities, where as in the case of non-TADF emitters index is closer to 1 indicating an enhanced overlap. 2CzPN and Cz2BP show a relatively higher trend indicating a compatibility with the previous examinations on twisting angle and singlet-triplet band gap. Additionally, the other TADF emitters have Φ_s indices closer to 0 demonstrating an efficient charge transfer as a result of well separated molecular orbitals.

The occupied and virtual Natural Transition Orbitals (NTOs) are depicted in Tables 4.7 - 4.10. A small overlap between molecular orbitals is observed for TADF materials. On the contrary, non-TADF emitters possess highly overlap occupied and virtual transition orbitals.

Table 4.7. Occupied and virtual NTO's for the TADF emitters (B3LYP/6-31+G(d), PCM in toluene) (1/2).

Compound	Occupied	Virtual
2CzPN	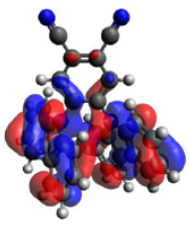	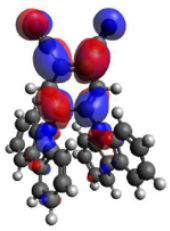
DMAC-DPS	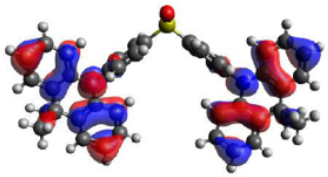	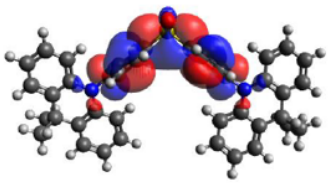
Cz2BP	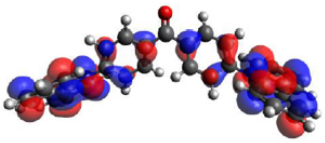	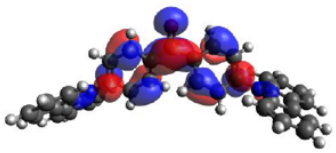
DMAC-TRZ	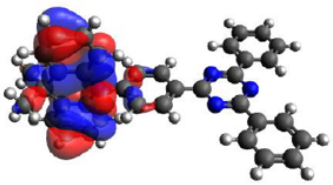	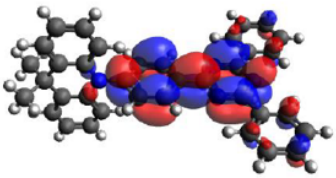

Table 4.8. Occupied and virtual NTO's for the TADF emitters (B3LYP/6-31+G(d), PCM in toluene) (2/2).

Compound	Occupied	Virtual
PXZPO	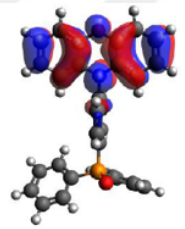	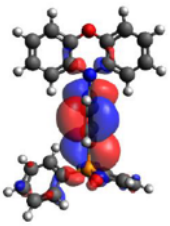
m-ATP-PXZ	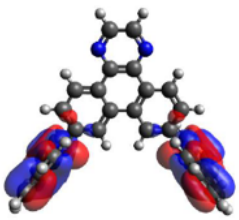	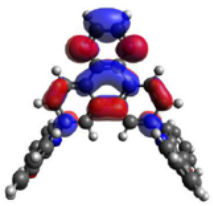
PXZ-PXB	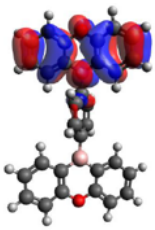	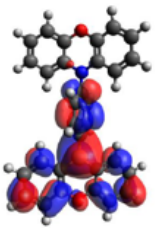

Table 4.9. Occupied and virtual NTO's for the non-TADF emitters (B3LYP/6-31+G(d), PCM in toluene) (1/2).

Compound	Occupied	Virtual
pCBP	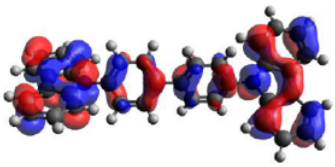	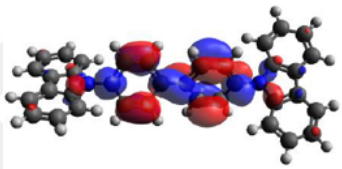
PhCz	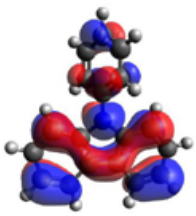	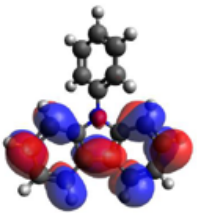
TPA	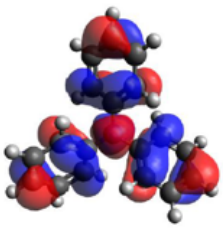	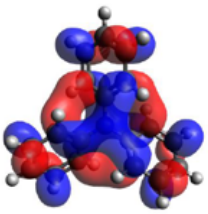
OX-DTT-Br	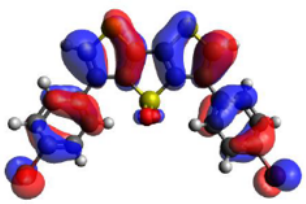	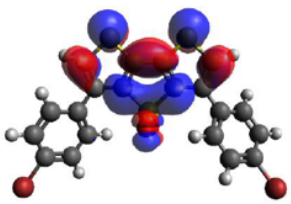

Table 4.10. Occupied and virtual NTO's for the non-TADF emitters (B3LYP/6-31+G(d), PCM in toluene) (2/2).

Compound	Occupied	Virtual
OX-DTT-F	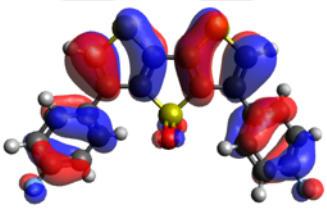	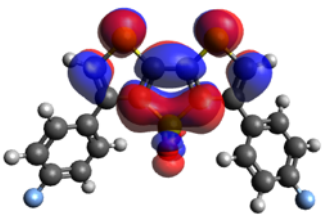
TPE		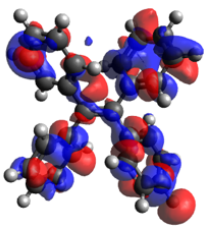
DTT-TPE	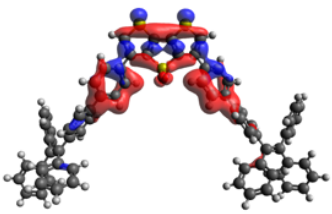	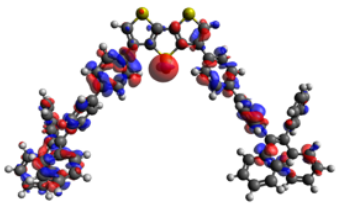

4.4.3. Excited State Profiles

The conversion between two electronic states that have same spin multiplicity is allowed in contrast to the transition among two distinct states with different spin multiplicity (S_1 and T_1) called as intersystem crossing (ISC) as shown in Figure 4.17 [67].

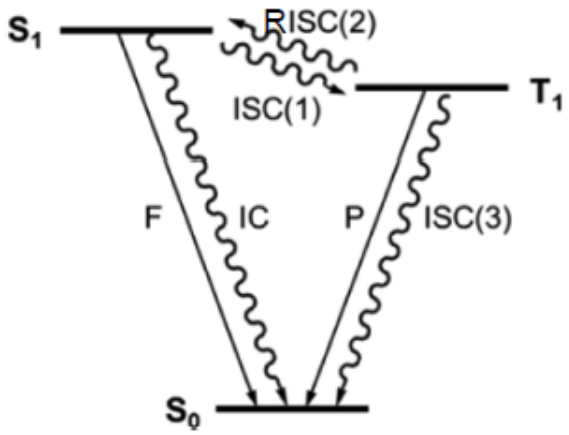

Figure 4.17. Jablonksi Diagram for a TADF emitter.

Since, the combination of intersystem crossing with reverse intersystem crossing plays a crucial role in effectiveness of TADF mechanism, it is important to employ singlet excited states and triplet excited states whose energy levels are extremely close to each other. The principal of TADF relies on an energy maintaining process that facilitates reverse intersystem crossing (k_{RISC}) in which triplet states are raised by thermal energy to a vibronic sub level that is isoenergetic with the emissive singlet states [68]. Accordingly, for an efficient TADF formation it is desired to have a high rate constant of reverse intersystem crossing (k_{RISC}) and it is obtained by lowering the gap between low lying charge transfer states. The k_{RISC} is exponentially proportional to the ratio of singlet-triplet band gap (ΔE_{S-T}) to temperature (T) where k_B is the Boltzmann constant [68].

$$k_{RISC} \propto \exp \frac{\Delta E_{S-T}}{k_B T} \tag{4.1}$$

Hence, to minimize (ΔE_{S-T}), since core structures of emitters are based on electron donating and accepting moieties, these groups can be adjusted by insertion of bridges also known as phenyl linkers which separates HOMO and LUMO leading to a small band gap. To achieve this goal, it is vital to choose donor and acceptor units with a suitable ionization potential (IP) together with electron affinity (EA) [68]. By the use of bipolar molecules with a large twisting angle between D and A units (a-type) shown in Figure 4.18, as mentioned in the previous section, a small exchange integral (J_{if}=1/2ΔE_{S-T}) for the S_1 transition that is associated with the orbital overlap integral can be achieved together with small ΔE_{S-T} [69]. However, in some cases, overlap splitting is not enough to stabilize charge-transfer leading to a decrease in quantum efficiency. Thence, with the insertion of an extra atomic bridge between D and A units (b-type) separation is achieved with a large fluorescence rate constant with an acceptable ΔE_{S-T} (Figure 4.18). Low singlet-triplet splittings can be produced by extending the spacer unit that connects the two adjacent D an A. However, the number and length of spacers incorporated should be chosen carefully because it may cause an isolation of molecular orbitals which blocks the charge transfer within the states.

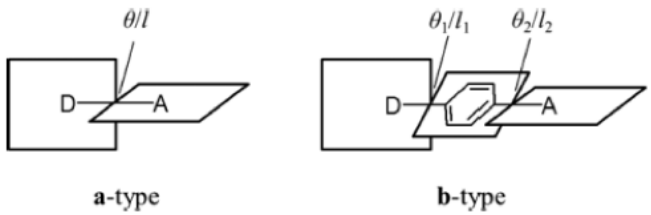

Figure 4.18. Designs of Donor-Acceptor and Donor-Bridge-Acceptor Models [66].

Table 4.11. Low lying singlet-triplet band gaps ΔE_{S-T} (eV) for TADF emitters (B3LYP/6-31+G(d), PCM in toluene).

Compound	**Calculated**	**Experimental**
2CzPN	0.24	0.31
DMAC-DPS	0.01	0.08
Cz2BP	0.19	0.21
DMAC-TRZ	0.01	0.04
PXZPO	0.02	0.26
***m*-ATP-PXZ**	0.01	0.04
PXZ-PXB	0.004	0.03

The calculated and experimental band gaps (ΔE_{S-T}) for TADF emitters are given in Table 4.11. The cyano-substituted emitters have enhanced electron affinity due to the powerful electron-withdrawing capacity of cyano groups. However, absence of a large steric hindrance and bulkiness between donor and acceptor groups in 2CzPN leads to a comparatively large (ΔE_{S-T}). In the diphenyl sulfoxide-based TADF emitter DMAC-DPS, has low singlet-triplet band gap with an effective reverse intersystem crossing (RISC) process. The superior TADF property of DMAC-DPS is because of the strong electron-withdrawing ability of diphenyl sulfoxide (DPS) moiety together with the powerful donor dimethyacridan (DMAC). Additionally, resulting orthogonal structure gives rise to a well aligned electronic density of the orbitals in the case of DMAC-DPS and DMAC-TRZ in which dimethylacridan was used as donor. Subsequently, DMAC-TRZ being one of the promising TADF emitters contains highly electron deficient triazine as electron accepting moiety with a low ΔE_{S-T}. Even though diphenyl ketone has a strong electron-withdrawing carbonyl group, Cz2BP has relatively high band gap in the absence of highly twisted conjugation. However, as Lee *et al*. reported [70] structures can be constructed in butterfly-shaped D-A-D types by substituting carbazole or phenoxazine as donor units to get an effective TADF emitter. In the following, TADF emitter PXZPO having phosphine oxide as weak acceptor,

shows high band gap experimentally. The diphenylphosphine group contributes to an augmented charge transport character. On the other hand, calculated (ΔE_{S-T}) values are not always compatible with experimental data. Contributions of the large π-conjugated system with a superior charge transport ability of *m*-ATP-PXZ that has three fused benzene rings with an electron-deficient core diaza-heterocyclic, is observed as low band gap. In the last emitter PXZ-PXB, twisted structure and strong donor ability of phenoxazine leads an efficient separation of HOMO and LUMO leading to a small (ΔE_{S-T}).

Table 4.12. Low lying singlet-triplet band gaps ΔE_{S-T} (eV) for non-TADF emitters (B3LYP/6-31+G(d), PCM in toluene).

Compound	**Calculated**	**Experimental**
pCBP	0.44	0.25
PhCz	0.62	0.25
TPA	0.42	-
DTT-Ox-Br	1.01	-
DTT-Ox-F	1.03	-
TPE	0.95	-
DTT-TPE	0.55	-

The ΔE_{S-T} values for non-TADF emitters that are comparatively higher than that of TADF emitter's due to the absence of orbital separation, are specified in Table 4.12. Consecutively, the impact of substituted moiety's electronegativity is examined by changing Br with F in dithienothiophene-*s*,*s*-dioxide derivatives, still ΔE_{S-T} is slightly different because of the inability of the terminal atom's to provide an extra torsion to the molecule. To clarify the effect of substituted moiety, DTT-TPE is modeled as a coupling product of dithienothiophene-*s*,*s*-dioxide and tetraphenylethylene (TPE). Thus, ΔE_{S-T} is lowered by implementing an extra steric hindrance with a high rotation to the molecule that separates frontier molecular orbitals relatively.

4.5. Conclusion

The study conducted in three phases has a main perspective to offer suitable emitter designs to be utilized in OLED structures. First, seven blue TADF emitters that have different groups of donor and acceptor moieties were selected to comprehend the effects of various building blocks in structures. After conformational examinations, the most stabilized geometries were taken for further excited state examinations and molecular orbitals were analyzed at different level of theories.

The most convenient designs belong to DMAC-DPS (sulfone-based), DMAC-TRZ (1,3,5-triazine-based), PXZ-PXB (boron-based), *m*-ATP-PXZ (1,4-diazatriphenylene) based emitters existed in highly twisted molecular forms. The calculated ΔE_{S-T} values of the emitters are compatible with the compiled experimental data and are relatively lower than those of non-TADF emitters. The Natural Transition Orbital (NTO) analyses predicted a minor overlap between ground and excited states and molecular orbital splitting can easily be visualized in Table 4.7 and Table 4.8 indicating that HOMO levels are populated in acceptor moieties where LUMO levels are mainly populated in donor groups. The Φ_s indices are close to 0 implying that an effective charge transfer occurs within the states.

Analyses performed on non-TADF molecules reveal a reduced molecular torsion with comparatively lower twisting angles associated with the overlapped frontier orbitals. Even though having an increased conjugation system, molecules suffer from high singlet-triplet splitting that suppresses RISC. The calculated Φ_s indices are close to 1 meaning that a local excited state nature of non-TADF emitters.

In order to induce intramolecular charge transfer, several design strategies have been proposed such as implementing a linker that enhances separation distance of donor and acceptor or substitution of an extra bulky group that enables rigidity to the structure which prevents molecular rotation. The aggregation induced emission character of a non-TADF emitter DTT-Ox was examined by inserting AIE fluoregen (TPE) and the results have shown a reduction in ΔE_{S-T} by 46% in DTT-TPE. How-

ever, the Natural Transition Orbital Analysis indicates that the Φ_s index of DTT-TPE is slightly smaller than that of DTT-Ox implying moderately large overlap between frontier orbitals giving rise to a non-effective charge transfer.

Consecutively, according to the desired improvements of properties and natures of OLED devices, one can adjust TADF emitter structures to be implemented on solid films. Following that, it is worth to underline the importance of the proper donor-acceptor choice. To have robust luminescence efficiency, system should contain molecular rigidity such as twist, bulky and spirojunction that present separated HOMO and LUMO. Also, it has been observed that even aggregation properties in solid states are crucial to realize effective luminescence.

5. FUTURE REMARKS

OLEDs that are constructed from TADF emitters possess improved device properties. On the other hand, to display an effective emission, TADF materials must be spread well into host matrices in order not to induce emission quenching and/or exciton annihilation. So that, a great majority of TADF doped OLEDs encounter with aforesaid problems [71].

Aggregation caused quenching issue associated with the formation of aggregates, can be eliminated by a distinctive photophysical phenomenon aggregation induced emission (AIE). Materials showing weak fluorescent characters in solutions with aggregation properties namely as AIEgens are used to increase fluorescence ability of materials in solid states. The emission quenching is reduced due to the twisted molecular nature of AIEgens that contain weakened intermolecular π - π interactions in aggregated state, this reduces the electronic coupling between building moieties together with frontier orbital overlap [72, 73].

Hereby, the effect of substituting a bulky moiety into a non-emissive molecule in solid phase, was investigated with computational methods. The substitution is achieved by the coupling between dithienothiophene$-s,s-$dioxide and tetraphenylethylene that is an archetypical AIE fluoregen, in which excited states are deactivated by non-radiation giving rise to non-emissive structure. The non-radiation is due to the dynamic intramolecular rotation of the multiple phenyl groups that rotate on the axes of σ-bonds connected to the central ethylene stator [74]. The restriction of intramolecular rotation (RIR) is observed in aggregated states due to the physical constrains, and this formation blocks the non-radiative relaxation with leading to radiative decay as shown in Figure 5.1.

TADF materials with aggregation induced natures are reported as incentivizing candidates possessing superb solid-state photoluminescence (PL) efficiencies with effectively utilized excitons [75].

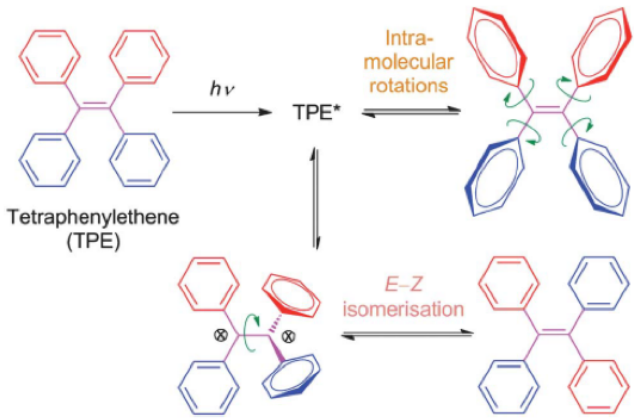

Figure 5.1. Intramolecular rotation affecting deactivation of excited TPE species [76].

A sharp decrease in ΔE_{S-T} promoted by well separated frontier orbitals demonstrated in Table 4.10 was noticed in DTT-TPE shown as 2D model in Figure 4.1 However, the observed band gap is not small enough to propagate RISC between triplet and excited states. Although the AIE strategy is promising when designing TADF materials to be doped in OLEDs, one should consider having reduced band gaps with twisted structures.

As future work, the packing patterns in crystal structures of TPE substituted molecules can be examined to be able to understand the mechanism of aggregation induced emission on delayed fluorescence and propose new TADF emitters.

REFERENCES

1. Bilen, K., O. Ozyurt, K. Bakırcı, S. Karslı, S. Erdogan, M. Yılmaz and O. Comaklı, "Energy production, consumption, and environmental pollution for sustainable development: A case study in Turkey", *Renewable and Sustainable Energy Reviews*, Vol. 12, No. 6, pp. 1529–1561, 2008.

2. Armeanu, D. Ş., G. Vintilă and Ş. C. Gherghina, "Does renewable energy drive sustainable economic growth? multivariate panel data evidence for EU-28 countries", *Energies*, Vol. 10, No. 3, p. 381, 2017.

3. Moldan, B., S. Janoušková and T. Hák, "How to understand and measure environmental sustainability: Indicators and targets", *Ecological Indicators*, Vol. 17, pp. 4–13, 2012.

4. Beça, P. and R. Santos, "Measuring sustainable welfare: A new approach to the ISEW", *Ecological Economics*, Vol. 69, No. 4, pp. 810–819, 2010.

5. Menegaki, A. N. and C. T. Tugcu, "Energy consumption and Sustainable Economic Welfare in G7 countries; A comparison with the conventional nexus", *Renewable and Sustainable Energy Reviews*, Vol. 69, pp. 892–901, 2017.

6. Menegaki, A. N. and A. K. Tiwari, "The index of sustainable economic welfare in the energy-growth nexus for American countries", *Ecological Indicators*, Vol. 72, pp. 494–509, 2017.

7. Hussain, A., S. M. Arif and M. Aslam, "Emerging renewable and sustainable energy technologies: State of the art", *Renewable and Sustainable Energy Reviews*, Vol. 71, pp. 12–28, 2017.

8. Ossai, C. I., "Optimal renewable energy generation–Approaches for managing ageing assets mechanisms", *Renewable and Sustainable Energy Reviews*, Vol. 72, pp.

269–280, 2017.

9. Beck, F. and E. Martinot, "Renewable energy policies and barriers", *Encyclopedia of Energy*, Vol. 5, No. 7, pp. 365–383, 2004.

10. Martinot, E., A. Chaurey, D. Lew, J. R. Moreira and N. Wamukonya, "Renewable energy markets in developing countries", *Annual Review of Energy and the Environment*, Vol. 27, No. 1, pp. 309–348, 2002.

11. Doman, L., K. Smith, P. Lindstrom, L. Mayne, J. Staub, E. Yucel, J. Barden, A. Fawzi, P. Martin, M. Mellish *et al.*, "International Energy Outlook 2006", *Energy Information Administration No. DOE/EIA-0484*, 2006.

12. Schott, M., "Introduction to the physics of organic electroluminescence", *Comptes Rendus de l'Académie des Sciences-Series IV-Physics*, Vol. 1, No. 4, pp. 381–402, 2000.

13. Im, Y., M. Kim, Y. J. Cho, J.-A. Seo, K. S. Yook and J. Y. Lee, "Molecular design strategy of organic thermally activated delayed fluorescence emitters", *Chemistry of Materials*, Vol. 29, No. 5, pp. 1946–1963, 2017.

14. Kalyani, N. T. and S. Dhoble, "Organic light emitting diodes: Energy saving lighting technology—A review", *Renewable and Sustainable Energy Reviews*, Vol. 16, No. 5, pp. 2696–2723, 2012.

15. Zhang, M., Z. Chen, L. Xiao, B. Qu and Q. Gong, "Optical design for improving optical properties of top-emitting organic light emitting diodes", *Journal of Applied Physics*, Vol. 113, No. 11, p. 113105, 2013.

16. Chen, A. C.-A., J. U. Wallace, S. K.-H. Wei, L. Zeng, S. H. Chen and T. N. Blanton, "Light-emitting organic materials with variable charge injection and transport properties", *Chemistry of Materials*, Vol. 18, No. 1, pp. 204–213, 2006.

17. Jin, J., W. Zhang, B. Wang, G. Mu, P. Xu, L. Wang, H. Huang, J. Chen and D. Ma, "Construction of high Tg bipolar host materials with balanced electron–hole mobility based on 1, 2, 4-thiadiazole for phosphorescent organic light-emitting diodes", *Chemistry of Materials*, Vol. 26, No. 7, pp. 2388–2395, 2014.

18. Wong, M. Y. and E. Zysman-Colman, "Purely organic thermally activated delayed fluorescence materials for organic light-emitting diodes", *Advanced Materials*, Vol. 29, No. 22, p. 1605444, 2017.

19. Baldo, M. A., D. O'brien, Y. You, A. Shoustikov, S. Sibley, M. Thompson and S. R. Forrest, "Highly efficient phosphorescent emission from organic electroluminescent devices", *Nature*, Vol. 395, No. 6698, p. 151, 1998.

20. Adachi, C., M. A. Baldo, M. E. Thompson and S. R. Forrest, "Nearly 100% internal phosphorescence efficiency in an organic light-emitting device", *Journal of Applied Physics*, Vol. 90, No. 10, pp. 5048–5051, 2001.

21. Zhang, Y., J. Lee and S. R. Forrest, "Tenfold increase in the lifetime of blue phosphorescent organic light-emitting diodes", *Nature Communications*, Vol. 5, p. 5008, 2014.

22. Jacquemin, D. and D. Escudero, "The short device lifetimes of blue PhOLEDs: insights into the photostability of blue Ir (III) complexes", *Chemical Science*, Vol. 8, No. 11, pp. 7844–7850, 2017.

23. Tao, Y., K. Yuan, T. Chen, P. Xu, H. Li, R. Chen, C. Zheng, L. Zhang and W. Huang, "Thermally activated delayed fluorescence materials towards the breakthrough of organoelectronics", *Advanced Materials*, Vol. 26, No. 47, pp. 7931–7958, 2014.

24. Zhang, Q., J. Li, K. Shizu, S. Huang, S. Hirata, H. Miyazaki and C. Adachi, "Design of efficient thermally activated delayed fluorescence materials for pure blue organic light emitting diodes", *Journal of the American Chemical Society*, Vol. 134, No. 36,

pp. 14706–14709, 2012.

25. Uoyama, H., K. Goushi, K. Shizu, H. Nomura and C. Adachi, "Highly efficient organic light-emitting diodes from delayed fluorescence", *Nature*, Vol. 492, No. 7428, p. 234, 2012.

26. Chen, D., X. Cai, X.-L. Li, Z. He, C. Cai, D. Chen and S.-J. Su, "Efficient solution-processed red all-fluorescent organic light-emitting diodes employing thermally activated delayed fluorescence materials as assistant hosts: molecular design strategy and exciton dynamic analysis", *Journal of Materials Chemistry C*, Vol. 5, No. 21, pp. 5223–5231, 2017.

27. Endo, A., K. Sato, K. Yoshimura, T. Kai, A. Kawada, H. Miyazaki and C. Adachi, "Efficient up-conversion of triplet excitons into a singlet state and its application for organic light emitting diodes", *Applied Physics Letters*, Vol. 98, No. 8, p. 42, 2011.

28. Cramer, C. J., *Essentials of computational chemistry: theories and models*, John Wiley & Sons, 2013.

29. Cohen, A. J., P. Mori-Sánchez and W. Yang, "Challenges for density functional theory", *Chemical Reviews*, Vol. 112, No. 1, pp. 289–320, 2011.

30. Burke, K., "Perspective on density functional theory", *The Journal of Chemical Physics*, Vol. 136, No. 15, p. 150901, 2012.

31. Kohn, W. and L. J. Sham, "Self-consistent equations including exchange and correlation effects", *Physical Review*, Vol. 140, No. 4A, p. A1133, 1965.

32. Leach, A. R. and A. Leach, *Molecular modelling: principles and applications*, Pearson education, 2001.

33. Elliott, P., F. Furche and K. Burke, "3 Excited States from Time-Dependent Den-

sity Functional Theory", *Reviews in Computational Chemistry*, Vol. 26, p. 91, 2009.

34. van Faassen, M. and K. Burke, "Time-dependent density functional theory of high excitations: to infinity, and beyond", *Physical Chemistry Chemical Physics*, Vol. 11, No. 22, pp. 4437–4450, 2009.

35. Marques, M. A. and E. K. Gross, "Time-dependent density functional theory", *A Primer in Density Functional Theory*, pp. 144–184, Springer, 2003.

36. Marques, M. A. and E. K. Gross, "Time-dependent density functional theory", *Annu. Rev. Phys. Chem.*, Vol. 55, pp. 427–455, 2004.

37. Chantzis, A., A. D. Laurent, C. Adamo and D. Jacquemin, "Is the Tamm-Dancoff approximation reliable for the calculation of absorption and fluorescence band shapes?", *Journal of Chemical Theory and Computation*, Vol. 9, No. 10, pp. 4517–4525, 2013.

38. Dreuw, A., J. L. Weisman and M. Head-Gordon, "Long-range charge-transfer excited states in time-dependent density functional theory require non-local exchange", *The Journal of Chemical Physics*, Vol. 119, No. 6, pp. 2943–2946, 2003.

39. Maitra, N. T., F. Zhang, R. J. Cave and K. Burke, "Double excitations within time-dependent density functional theory linear response", *The Journal of Chemical Physics*, Vol. 120, No. 13, pp. 5932–5937, 2004.

40. Elliott, P., S. Goldson, C. Canahui and N. T. Maitra, "Perspectives on double-excitations in TDDFT", *Chemical Physics*, Vol. 391, No. 1, pp. 110–119, 2011.

41. Fetter, A. L. and J. D. Walecka, *Quantum theory of many-particle systems*, Courier Corporation, 2012.

42. Grüning, M., A. Marini and X. Gonze, "Exciton-plasmon states in nanoscale ma-

terials: breakdown of the Tamm- Dancoff approximation", *Nano Letters*, Vol. 9, No. 8, pp. 2820–2824, 2009.

43. Bai, Z., J. Demmel, J. Dongarra, A. Ruhe and H. van der Vorst, *Templates for the solution of algebraic eigenvalue problems: a practical guide*, SIAM, 2000.

44. McWeeny, R., *Methods of molecular quantum mechanics*, Academic press, 1992.

45. de la Vega, J. G. and B. Miguel, "Basis sets for computational chemistry", *Introduction to Advanced Topics of Computational Chemistry, edited by LA Montero, LA Dıaz, and R. Bader*, pp. 41–80.

46. Pople, J. A. and W. J. Hehre, "Computation of electron repulsion integrals involving contracted Gaussian basis functions", *Journal of Computational Physics*, Vol. 27, No. 2, pp. 161–168, 1978.

47. Binkley, J. S., J. A. Pople and W. J. Hehre, "Self-consistent molecular orbital methods. 21. Small split-valence basis sets for first-row elements", *Journal of the American Chemical Society*, Vol. 102, No. 3, pp. 939–947, 1980.

48. Hertsen, D., *Modeling the reactivity and selectivity of chemical reactions with advanced molecular modeling methods*, Ph.D. Thesis, Ghent University, 2017.

49. Tomasi, J., B. Mennucci and R. Cammi, "Quantum mechanical continuum solvation models", *Chemical Reviews*, Vol. 105, No. 8, pp. 2999–3094, 2005.

50. Barone, V., M. Cossi and J. Tomasi, "Geometry optimization of molecular structures in solution by the polarizable continuum model", *Journal of Computational Chemistry*, Vol. 19, No. 4, pp. 404–417, 1998.

51. Barone, V. and M. Cossi, "Quantum calculation of molecular energies and energy gradients in solution by a conductor solvent model", *The Journal of Physical Chemistry A*, Vol. 102, No. 11, pp. 1995–2001, 1998.

52. Etienne, T., X. Assfeld and A. Monari, "Toward a quantitative assessment of electronic transitions' charge-transfer character", *Journal of Chemical Theory and Computation*, Vol. 10, No. 9, pp. 3896–3905, 2014.

53. Etienne, T., X. Assfeld and A. Monari, "New insight into the topology of excited states through detachment/attachment density matrices-based centroids of charge", *Journal of Chemical Theory and Computation*, Vol. 10, No. 9, pp. 3906–3914, 2014.

54. Bruhn, G., E. R. Davidson, I. Mayer and A. E. Clark, "Löwdin population analysis with and without rotational invariance", *International Journal of Quantum Chemistry*, Vol. 106, No. 9, pp. 2065–2072, 2006.

55. Reed, A. E., R. B. Weinstock and F. Weinhold, "Natural population analysis", *The Journal of Chemical Physics*, Vol. 83, No. 2, pp. 735–746, 1985.

56. Gross, K. C., P. G. Seybold and C. M. Hadad, "Comparison of different atomic charge schemes for predicting pKa variations in substituted anilines and phenols", *International Journal of Quantum Chemistry*, Vol. 90, No. 1, pp. 445–458, 2002.

57. Ozturk, T., E. Ertas and O. Mert, "Dithienothiophenes", *Tetrahedron*, Vol. 47, No. 61, pp. 11055–11077, 2005.

58. Shizu, K., H. Tanaka, M. Uejima, T. Sato, K. Tanaka, H. Kaji and C. Adachi, "Strategy for designing electron donors for thermally activated delayed fluorescence emitters", *The Journal of Physical Chemistry C*, Vol. 119, No. 3, pp. 1291–1297, 2015.

59. Zhao, Y. and D. G. Truhlar, "The M06 suite of density functionals for main group thermochemistry, thermochemical kinetics, noncovalent interactions, excited states, and transition elements: two new functionals and systematic testing of four M06-class functionals and 12 other functionals", *Theoretical Chemistry Accounts*, Vol. 120, No. 1-3, pp. 215–241, 2008.

60. Wodrich, M. D., C. Corminboeuf and P. v. R. Schleyer, "Systematic errors in computed alkane energies using B3LYP and other popular DFT functionals", *Organic Letters*, Vol. 8, No. 17, pp. 3631–3634, 2006.

61. Etienne, T., "Probing the locality of excited states with linear algebra", *Journal of Chemical Theory and Computation*, Vol. 11, No. 4, pp. 1692–1699, 2015.

62. Frisch, M. J., G. Trucks, H. B. Schlegel, G. Scuseria, M. Robb, J. Cheeseman, G. Scalmani, V. Barone, B. Mennucci, G. Petersson *et al.*, "Gaussian 09, revision A. 1", *Gaussian Inc. Wallingford CT*, Vol. 27, p. 34, 2009.

63. Yang, Z., Z. Mao, Z. Xie, Y. Zhang, S. Liu, J. Zhao, J. Xu, Z. Chi and M. P. Aldred, "Recent advances in organic thermally activated delayed fluorescence materials", *Chemical Society Reviews*, Vol. 46, No. 3, pp. 915–1016, 2017.

64. Bâldea, I., "Floppy molecules as candidates for achieving optoelectronic molecular devices without skeletal rearrangement or bond breaking", *Physical Chemistry Chemical Physics*, Vol. 19, No. 45, pp. 30842–30851, 2017.

65. Wang, K., C.-J. Zheng, W. Liu, K. Liang, Y.-Z. Shi, S.-L. Tao, C.-S. Lee, X.-M. Ou and X.-H. Zhang, "Avoiding Energy Loss on TADF Emitters: Controlling the Dual Conformations of D–A Structure Molecules Based on the Pseudoplanar Segments", *Advanced Materials*, Vol. 29, No. 47, p. 1701476, 2017.

66. Masunov, A. E. and I. A. Mikhailov, "Theory and computations of two-photon absorbing photochromic chromophores", *European Journal of Chemistry*, Vol. 1, No. 2, pp. 142–161, 2010.

67. Turro, N. J., V. Ramamurthy and J. C. Scaiano, "Modern molecular photochemistry of organic molecules", *Photochemistry and Photobiology*, Vol. 88, No. 4, pp. 1033–1033, 2012.

68. Santos, P. L., J. S. Ward, P. Data, A. S. Batsanov, M. R. Bryce, F. B. Dias

and A. P. Monkman, "Engineering the singlet–triplet energy splitting in a TADF molecule", *Journal of Materials Chemistry C*, Vol. 4, No. 17, pp. 3815–3824, 2016.

69. Zhang, Q., H. Kuwabara, W. J. Potscavage Jr, S. Huang, Y. Hatae, T. Shibata and C. Adachi, "Anthraquinone-based intramolecular charge-transfer compounds: computational molecular design, thermally activated delayed fluorescence, and highly efficient red electroluminescence", *Journal of the American Chemical Society*, Vol. 136, No. 52, pp. 18070–18081, 2014.

70. Lee, S. Y., T. Yasuda, Y. S. Yang, Q. Zhang and C. Adachi, "Luminous Butterflies: Efficient Exciton Harvesting by Benzophenone Derivatives for Full-Color Delayed Fluorescence OLEDs", *Angewandte Chemie International Edition*, Vol. 53, No. 25, pp. 6402–6406, 2014.

71. Hong, Y., J. W. Lam and B. Z. Tang, "Aggregation-induced emission", *Chemical Society Reviews*, Vol. 40, No. 11, pp. 5361–5388, 2011.

72. Guo, J., X.-L. Li, H. Nie, W. Luo, S. Gan, S. Hu, R. Hu, A. Qin, Z. Zhao, S.-J. Su *et al.*, "Achieving High-Performance Nondoped OLEDs with Extremely Small Efficiency Roll-Off by Combining Aggregation-Induced Emission and Thermally Activated Delayed Fluorescence", *Advanced Functional Materials*, Vol. 27, No. 13, p. 1606458, 2017.

73. Fan, J., L. Lin and C.-K. Wang, "Excited state properties of non-doped thermally activated delayed fluorescence emitters with aggregation-induced emission: a QM/MM study", *Journal of Materials Chemistry C*, Vol. 5, No. 33, pp. 8390–8399, 2017.

74. Tseng, N.-W., J. Liu, J. C. Ng, J. W. Lam, H. H. Sung, I. D. Williams and B. Z. Tang, "Deciphering mechanism of aggregation-induced emission (AIE): Is E–Z isomerisation involved in an AIE process?", *Chemical Science*, Vol. 3, No. 2, pp. 493–497, 2012.

75. Yu, L., Z. Wu, G. Xie, W. Zeng, D. Ma and C. Yang, "Molecular design to regulate the photophysical properties of multifunctional TADF emitters towards high-performance TADF-based OLEDs with EQEs up to 22.4% and small efficiency roll-offs", *Chemical Science*, Vol. 9, No. 5, pp. 1385–1391, 2018.